

# Interim report of plasma catalysis: Footprints in the past and blueprints for the future

Hyun-Ha Kim<sup>1,\*</sup>, Ayman A Abdelaziz<sup>1,2</sup>, Yoshiyuki Teramoto<sup>1</sup>, Tomohiro Nozaki<sup>3,\*</sup>, Karol Hensel<sup>4</sup>,  
Young-Sun Mok<sup>5</sup>, Shirjana Saud<sup>5</sup>, Duc Ba Nguyen<sup>5,6</sup>, Dae Hoon Lee<sup>7</sup>, Woo Seok Kang<sup>7</sup>

<sup>1</sup> Environmental Management Research Institute, National Institute of Advanced Industrial Science and Technology (AIST), 16-1 Onogawa Tsukuba, Ibaraki 3058569, Japan

<sup>2</sup> Physics Department, Assiut University, Assiut 71516, Egypt

<sup>3</sup> Department of Mechanical Engineering, Tokyo Institute of Technology, O-Okayama, Tokyo, Japan

<sup>4</sup> Department of Environmental Physics, Comenius University, Bratislava, Slovakia

<sup>5</sup> Department of Chemical Engineering, Jeju National University, Jeju, Korea

<sup>6</sup> Institute of Research and Development, Duy Tan University, Danang 550000, Vietnam

<sup>7</sup> Department of Plasma Engineering, Korea Institute of Machinery and Materials (KIMM), Daejeon 34103, Korea

\* Corresponding author: [hyun-ha.kim@aist.go.jp](mailto:hyun-ha.kim@aist.go.jp) (Hyun-Ha Kim), [nozaki.t.ab@m.titech.ac.jp](mailto:nozaki.t.ab@m.titech.ac.jp) (Tomohiro Nozaki)

Received: 22 February 2021

Revised: 4 March 2021

Accepted: 5 March 2021

Published online: 8 March 2021

## Abstract

Interactions at the interface of the plasma and catalyst surface have the potential to open new chemical pathways that have never been realized with conventional plasma alone or catalyst-only processes. Plasma catalysis is now facing a rapid growth phase after a long, gradual period of growth over several decades. This interim report aims to analyze the progress of plasma catalysis over the last two decades and provide some future challenges. For readers who are laymen in this field, a brief explanation of plasma catalysis is provided in the introduction. The first part of the interim report addresses five important matching issues for plasma and one for catalyst. We also collectively present experimental evidence in the literature that underpins the interaction of plasma with a catalyst that is directly inserted into the plasma zone. We also emphasize on synergy, which is sometimes mistreated by neglecting the heating effect under a high energy input. In the second part of this report, we discuss recent achievements. A brief review of the historical development of plasma reactors from a packed-bed to a honeycomb discharge, which is suitable for large-scale applications, is provided. In the final part, some blueprints for future challenges are delineated based on the experimentally observed evidence from macro- to nano- and atomic-scale measurements. Developing effective catalysts capable of utilizing vibrationally excited hot molecules will be key for forthcoming innovations in plasma catalysis. We also underline the importance of implementing new sets of materials (both metals and supports) by introducing recent notable examples in conventional catalysis. The interlink between computational works on the macro/micro-scale and molecular/atomic-scale will be an interesting task in the future.

**Keywords:** Plasma catalysis, matching, synergy, operando measurement, vibrational excitation, reactor design.

## 1. Introduction

In nonthermal plasma (NTP) chemistry, the presence of energetic electrons induces various chemical reactions even at ambient temperature and atmospheric pressure. The collision of energetic electrons with gas molecules produces highly reactive chemical species, which play key roles in plasma chemistry. High reactivity often suffers from low reaction selectivity, which leads to high energy consumption and the formation of unwanted byproducts. These experiences in the 1990s led researchers to look at the combination of plasma with a catalyst.

Plasma catalysis is becoming recognized as an emerging type of chemical process [1]. In recent years, many scientific conferences have prepared plasma catalysis as one of the session topics. The complexity of interactions between NTP and catalyst is far beyond our expectations, which has been made obvious by intensive studies in the last two decades [2]. As similar topics dealing with interactions between plasma and a

solid surface, atomic layer etching (ALE), atomic layer deposition (ALD), and plasma-enhanced chemical vapor deposition (PE-CVD) have been studied. An extensive database was established on the optimum plasma parameters for a desired surface change. An information link between these the past works and currently ongoing plasma catalysis works may be necessary to establish similarities and differences. Fundamental aspects of plasma catalysis, the reason why the combination is necessary, how the two parts can be combined, and the expected merits have been discussed in a number of reviews and books [3-6].

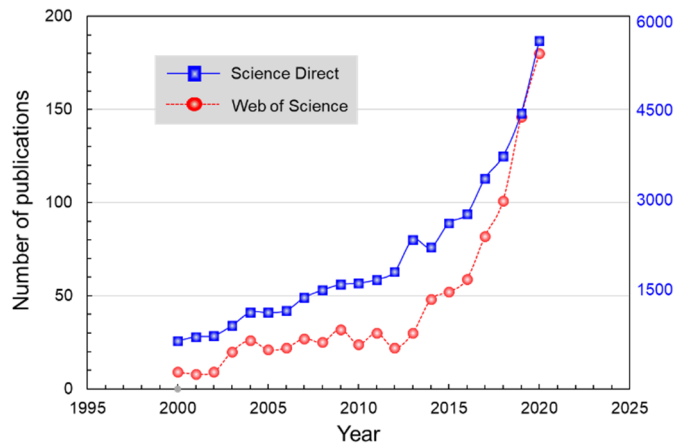


**Fig. 1.** Number of publications on plasma catalysis, obtained with the keywords “Plasma AND catal\*” in ISI Web of Science (title only) and “plasma catalysis” in Science Direct (all fields).

Fig. 1 shows the annual trend in the number of publications on plasma catalysis. Aside from the difference in the number of publications, a rapid increase was observed after 2010. The combination of plasma and a catalyst, albeit sporadically, has been considered before 2000 for NO<sub>x</sub> removal [7-9], methane conversion [10, 11], CO<sub>2</sub> hydrogenation [12], catalyst pretreatment for CO oxidation [13], and ammonia synthesis [14]. The increasing pattern indicates that the plasma catalysis has transitioned from the startup phase to the rapid growth phase. The main objective of this interim report is to briefly review past achievements in plasma catalysis, and to share common challenges for further development of this topic. We also provide some critique of synergy in plasma catalysis that has been mistreated in some cases. This report does not deal with the details of the applications of plasma catalysis, because a number of reviews and articles are available for volatile organic compound (VOC) removal [15, 16], NO<sub>x</sub> removal [17], CO<sub>2</sub> dry reforming [5, 18], and NH<sub>3</sub> synthesis [19, 20]. A broader perspective that links with the general behavior of plasma catalysis is discussed for both past achievements and necessary steps for forthcoming developments.

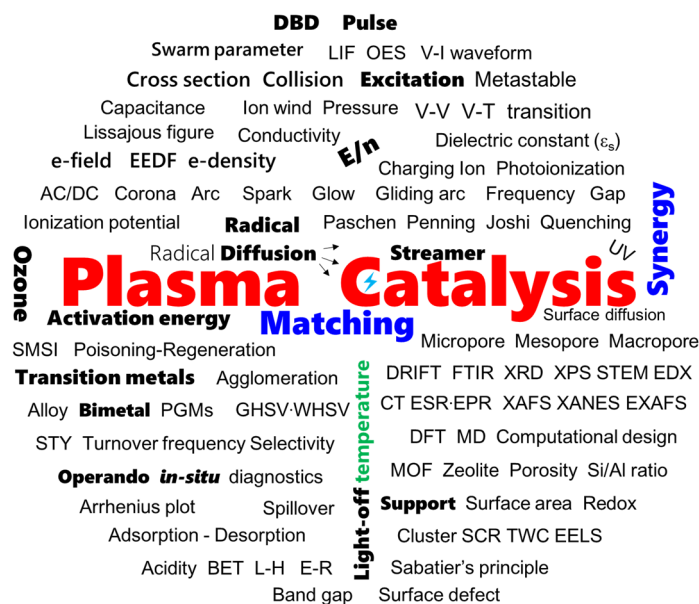


**Fig. 2.** Important keywords in plasma catalysis widely found in the literature.

Fig. 2 summarizes the general keywords of plasma catalysis. Each plasma and catalyst possess various parameters to be considered. In particular, some of the essential topics given in bold letters are emphasized in this interim report. Catalysts consist of supports and active metals. A support has a high surface area ( $10^2\sim 10^3\text{ m}^2\text{ g}^{-1}$ ) to which the active metal nanoparticles (NPs) are fixed. A proper combination of active metals and support has been the key issue of catalysis in the past. For a given set of metals and supports, the catalytic performance is also affected by the loading amount, size of metal NPs, preparation method, and dispersion. Matching between the plasma and catalyst requires new sets of perspectives to realize the synergistic effect, the details of which are discussed in Section 2.1. The dynamics of the surface streamer are also important aspect in understanding the combined effect. Development of effective catalysts that can utilize electronically and vibrationally excited molecules at the surface of a catalyst is one of key issues in plasma catalysis. Matching the right material requires many new steps of development. In one sense, this matching can only be effective under intensive collaboration between material science, plasma, catalysts, and analytical instruments. We hope that this paper will draw attention from many different fields and extend these collaborations.

## 2. Fundamentals of plasma catalysis

The combination of NTP and a catalyst pursues a performance that exceeds that of the NTP alone process in terms of energy efficiency and product selectivity. Catalysts are only active when the temperature condition, known as light-off temperature, is satisfied. Lowering the light-off temperature has long been the goal of most catalytic reactions. Basically, low temperature and catalytic activity are incompatible within conventional thermal catalysis. In contrast, low-temperature operation is one of the distinctive characteristics of NTP. The presence of NTP enables catalysts to work effectively at temperatures far below the light-off temperature. The effect of plasma on catalysis is multidisciplinary. The presence of a catalyst can also change the plasma properties, such as the plasma mode and local densities of electrons and radicals. This section describes the five matching issues and critiques of synergy.

### 2.1 Five important matchings

Matching is an essential design strategy for ensuring beneficial interactions between the plasma and the catalyst. Of course, proper matching should avoid both undermatching and overmatching. Fig. 3 schematically summarizes the matching parameters that should be carefully considered when designing a plasma–catalyst system. Four types of matching are addressed for the plasma and one for the catalyst. Plasma chemistry involves the six main particles of electrons, photons (i.e., ultraviolet (UV)), atoms, excited molecules, and positive and negative ions, regardless of the reactions and applications [21]. Plasma catalysis is the combined interaction of these six particles with the surface. As an additional but indispensable effect, plasma produces electrohydrodynamic flow (EHD), electric field, and heat. In particular, the heating effect can no longer be negligible when the specific input energy is high. Thermal plasma relies mostly on heat [22]. However, heat should also be carefully dealt with when using NTP. Plasma chemistry and heterogeneous catalysis are multidisciplinary fields involving electrical engineering, chemical engineering, physical chemistry, material science, computational science, instrumental analysis, and organic/inorganic chemistry. Intensive matching of researchers from different fields will be highly important in the future.

#### 2.1.1 Species matching (what)

Species matching usually requires the control of the gas mixture, which is beneficial for catalytic reactions. For example, controlling oxygen and water vapor is necessary to provide reactive oxygen species (ROS) for oxidation. The reduction process should be coupled with reactive nitrogen species (RNS) or hydrogen. Electrons play an essential role in both the plasma dynamics and catalytic reactions. Electron transfer from metal NPs to the antibonding orbital of adsorbed or impinging molecules can enhance bond breaking. The mobility of electrons is 500 times larger than that of most ions owing to their small mass. If plasma is generated in the surface streamer mode, electrons can arrive at the surface. However, electrons in gas-phase are trapped by electronegative molecules ( $\text{H}_2\text{O}$ ,  $\text{O}_2$ ,  $\text{CO}_2$ ) within  $10^{-8}\sim 10^{-7}$  s, and ions can be the main form of charge available on the surface. Density functional theory (DFT) calculations by Bal *et al.* [23] showed that a negatively charged surface can promote the splitting of  $\text{CO}_2$ , and the reactivity of transition metals may be

controllable. Similarly, Hyman and Medlin indicated that a positively charged surface reduces the adsorption energies of O species on Pt(111), whereas a negatively charged surface increases adsorption [24]. The other expected effects of these electrons and ions are charging and neutralization with opposite charges. Local charging and the resulting electric field can induce electron emission (field emission) and charge transfer. Ions also arrive at the surface in many ways. Ions are left behind the track of the surface streamer. Positive ions may preferentially neutralize near the metal surface, where abundant electrons are available. Depending on the internal energy state of the ions, dissociative recombination can occur at the surface where it collides. If these processes can be realized under proper control, new sets of catalytic reactions may be possible. Excited molecules are also interesting components of the plasma. Electronically excited species usually decay to the ground state, accompanied by light emission. Their typical relaxation times are of the order of  $\sim 10^{-7}$  s, and thus, they are less likely to reach the surface before deactivation. Vibrational energy is an interesting topic in surface chemistry. Molecular beam experiments have demonstrated its significant contribution in terms of dissociative adsorption, sticking probability, and surface accommodation. A detailed discussion is provided in Section 4.3.

### 2.1.2 Flux matching (how much)

Flux matching is related to the mole fraction, which must be converted. The higher the target value, the more flux is required. Plasma chemistry is often controlled by the specific input energy (SIE), which is the ratio of discharge power to gas flow rate, as given in Eq. (1). A variety of different names (specific energy input, energy density, input energy density) and units ( $\text{J L}^{-1}$ ,  $\text{Wh Nm}^{-3}$ ,  $\text{eV molecule}^{-1}$ ) have been coined, but the main concept is identical.

$$\text{Specific input energy} = \frac{\text{discharge power}}{\text{gas flow rate}} = \frac{P_{dis}}{Q} \quad (1)$$

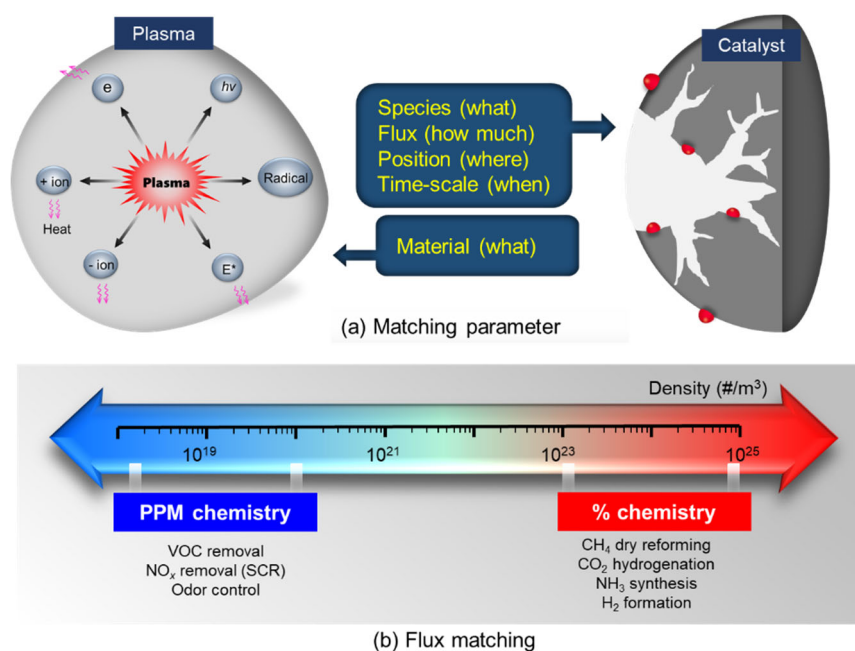


**Fig. 3.** Matching between plasma and catalyst: (a) matching parameter, (b) flux matching.

SIE is a useful knob for tuning the flux of reactive species from plasma. The first mention of SIE may date back to the 1960s (see [25] and references therein), when it was explicitly described as “*specific energy is the significant parameter for comparing results of experiments carried out in different reactors.*”. The same concept, albeit with different names (specific energy, power density, or specific corona power), has also been used in electrostatic precipitators [26–28]. “More reaction with less energy input” has been the ultimate goal of every form of plasma chemistry. “Much less” in plasma catalysis may include “less catalytic materials” but energy consumption has to be ranked as a higher priority. As shown in Fig. 3 (b), most environmental applications deal with pollutants at the parts per million (ppm) level, herein referred to as PPM chemistry.

Many NTP reactors intrinsically produce ROS/RNS at the  $10^1$ – $10^2$  ppm level which is consistent with most environmental applications. In other words, there exists a natural flux matching of plasma species to PPM chemistry. This is one of the reasons why some large scale applications were achieved more than 10 years ago [29]. Atmospheric-pressure plasma jets using He or Ar as carriers also belong to PPM chemistry. Ono *et al.* measured the flux of ROS in a He plasma jet to be in the range of  $\sim 10^{-13}$  cm $^{-3}$  [30]. The role of UV, emitted from discharge in an air-like mixture, has long been a subject of controversy. Currently, the UV contribution to plasma chemistry is considered to be negligible not because of the photocatalytic reaction but because of its low UV flux. Quantitative measurements of UV flux in air plasma by several groups revealed that it is only on the order of several  $\mu\text{W cm}^{-2}$ , which is approximately three orders of magnitude less than that of outdoor solar UV flux (2–5 mW cm $^{-2}$ ) [31]. It should be noted that an external light source with sufficient UV flux can improve the performance of plasma catalysis [32–34].

However, most energy-related applications (ammonia synthesis, hydrogen production, methane reforming, and CO $_2$  hydrogenation) require high mole fractions to be reacted. To meet the requirement, the flux of reactive species should be increased to the parts per hundred (PPH) level, which is simply referred to as “PPH (percent) chemistry” in this paper. Increasing the applied voltage and frequency (i.e., high input power) is the first option for plasma to provide a higher radical flux. However, a higher energy input is a drawback of plasma for practical applications on a mass production scale.

### 2.1.3 Position matching (where)

Position matching is the effective distance between the plasma and the surface of the catalyst to ensure mutual interaction. Chemical reactions between a plasma and catalyst depend primarily on the mass transfer of radicals between the interface of the plasma and the catalyst surface. For better use of short-lived chemical species, the distance between the plasma and the surface is important. The dimensionless parameter  $\Lambda$  describes the interaction criteria between the reactive species and the catalyst [31].

$$\Lambda = \frac{L_l}{L_D} \leq 1 \quad (2)$$

$L_D$  and  $L_l$  indicate the diffusion length of the reactive species, and the distance between the plasma and catalyst, respectively. The diffusion length ( $L_D$ ) is limited by the reactivity of the plasma species. Under atmospheric pressure, the two-dimensional  $L_D$  is approximately 60  $\mu\text{m}$ . If the plasma is generated at a distance beyond  $L_D$  interactions of radicals with the catalyst can hardly occur. Recently, Nozaki *et al.* experimentally observed that plasma-induced oxidation of Ni into NiO occurs within 20  $\mu\text{m}$  [35], which is consistent with this estimation. The parameter  $\Lambda$  can also be applied to other plasma processes such as sterilization, plasma medicine and surface treatment. A shorter  $L_l$  will increase the chances of interaction between the plasma and the target materials (i.e., the catalyst in the case of plasma catalysis).

Some ROS have a long lifetime, so they can be utilized even downstream of the plasma reactor. Ozone-assisted catalysis (OAC) is one good example of this strategy [36–38]. Heat from the plasma can also be utilized in the subsequent catalyst bed depending on the distance between the plasma zone and the catalyst bed.

### 2.1.4 Time-scale matching (when)

Chemical reactions in plasma can be considered a three-step process. The first step is radical formation on the course of the discharge channel (streamer or microdischarges) within  $10^{-9}$ – $10^{-7}$  s $^{-1}$ . The second step is fast radical reaction, which has a typical time-scale of  $10^{-5}$ – $10^{-4}$  s. Some radicals recombine to form relatively stable molecules, such as O $_3$ , and H $_2$ O $_2$ , which can finally induce slow reactions even outside the plasma reactor. Diffusion is an obvious example of different timescales between the plasma and catalyst. Diffusion coefficients in gas-phase are in the  $10^{-1}$  cm $^2$  s $^{-1}$  range: O = 0.27 cm $^2$  s $^{-1}$ , O = 0.21 cm $^2$  s $^{-1}$ , and O $_3$  = 0.1–0.2 cm $^2$  s $^{-1}$ . The diffusion on the surface is a function of temperature ( $D = D_0 e^{-E_a/k_B T}$ ) and the typical values are in the range of  $10^{-4}$ – $10^{-9}$  cm $^2$  s $^{-1}$ , which is several orders of magnitude smaller than those in the gas phase. The catalytic turnover timescale is known to be in the range of  $10^{-2}$ – $10^2$  s $^{-1}$  [39]. Somorjai postulated that surface reconstruction may be associated with the turnover time-scale. Bal and Neyts reported a collective variable-driven hyperdynamics (CVHD) method for modeling CH $_4$  reaction on surfaces [40]. For CH $_4$  decomposition on Ni(111) at 800 K, elementary reactions ranged from rather fast step such as dissociation of a C–H bond ( $\sim$

50 ps), to the slow decomposition of adsorbed  $\text{CH}_x$  (0.1 ms). One possibility to bridge the large time-scale gap between the plasma and the catalyst is adsorption. Isotopically labelled probe ( $^{18}\text{O}_2$ ) experiments [41] and chemical titration [42–47] methods revealed that oxygen or nitrogen species can be survived on the surfaces long time. For example, oxygen species fixed on Ag NPs can survive for over 10 h, even retaining their chemical activity for CO or NO oxidation. Despite the experimental evidence on plasma-induced surface fixation, the exact forms on the surface are still unknown.

When vibrationally excited molecules collide with the surface, vibrational energy is used for either local heating or endothermic energy for the chemisorption of incident molecules. Metal NPs can be heated within  $10^{-9}$  s, but their contribution to catalytic reactions is questionable because they also exhibit the rapid cooling. This timescale does not match the typical catalytic turnover frequency. Another important issue is the energy released via charge recombination on the catalyst surface. This is a well-known phenomenon in plasma-enhanced gas-phase NP synthesis [48, 49]. Moreover, induction heating of NPs, and supported nanostructures [50] caused by the high-frequency electric field (kHz to MHz) has a negligible effect. Although temperature increase at the molecular scale is difficult to identify, such energy can modify the adsorbed surface species that induce unique plasma-induced reaction pathways.

### 2.1.5 Material matching (what)

Most catalysts consist of nanometer-sized active metals ( $M = \text{Ag, Cu, Mn, Fe, Ni, Pd, Pt, Rh, Ru}$  etc.) dispersed on high-surface area supports ( $\text{TiO}_2$ ,  $\gamma\text{-Al}_2\text{O}_3$ ,  $\text{SiO}_2$ ,  $\text{CeO}_2$ , metal-organic frameworks (MOF), or zeolites). Unsupported metal catalysts are exceptional, but have also received increasing attention [51, 52]. The performance of a given metal differs depending on the support on which the material component is dispersed. In particular, the atomic- and nano-scale interfaces of metal NPs and supports play an important role in the dynamics of metal NPs and catalytic reactions. Material matching can be simplified to what types of catalyst can work well in a plasma environment and how they can be found through experiments and modeling.

From the authors' experience over the last 20 years, it is clear that not all catalysts can be effective in a plasma environment. A substantial increase, so-called synergy, is only possible when plasma is matched with a proper combination of gases, catalysts, and heating conditions. Precious metals, such as platinum group metals (PGMs), have been widely used in many catalytic processes because of their high activity, stability, and selectivity. PGMs are used most notably for environmental catalysts, including exhaust gas cleaning in automobiles. Replacing PGMs with ubiquitous materials remains challenging. The myriad applications of PGMs (Ru, Rh, Pd, Pt, Ir, and Os) also indicate a huge potential impact on industry if sustainable alternatives are developed. Considering the extensive studies over several decades in material science and catalysis, advances in substituting PGMs with cost-effective abundant materials are still limited. Most importantly, it is usually difficult to exceed the extraordinary performance of PGMs with alternative metals. Nevertheless, several interesting findings have been reported, especially for bimetallic catalysts. For example, Kusada *et al.* synthesized Pd–Ru solid–solution–alloy NPs for  $\text{H}_2$  storage and CO oxidizing ability [53]. The Pd–Ru solid–solution–alloy NPs exhibited higher CO conversion than a Pd or Rh catalyst alone, and the optimum ratio was found at Pd/Ru = 1. These new materials may have high potential when combined with NTPs.

It is worth mentioning that “activity inversion” is observed between thermal and plasma catalysis. What works well in thermal catalysis does not guarantee the same performance in plasma catalysis. Fig. 4 shows an example in which the activity is reversed from thermal catalysis to OAC for CO oxidation on a bimetallic Ag–Pd catalyst [54]. In thermal catalysis, the order of CO conversion was Pd–LaFeO<sub>3</sub> > Pd–Cu > Pd > Pd–Mn > Pd–Fe > Ag–Pd at 200 °C, which is almost the reverse order of that of OAC. *In situ* Fourier transform infrared (FTIR) measurements revealed that the cooperative effect in the Ag–Pd catalyst involved modification of CO adsorption and the suppression of intermediate accumulation [54]. High-angle annular dark field (HAADF) images and energy-dispersive X-ray spectroscopy (EDS) measurements confirmed the proximity of the two active components (Ag and Pd), which was essential for the cooperative interaction. According to the X-ray absorption near edge structure (XANES) measurement of a Pd–Ag/ $\gamma\text{Al}_2\text{O}_3$  catalyst by Huang *et al.* [55], the Pd d-band electron density increased in the presence of Ag. Similar activity inversions have been reported for single-stage and two-stage configurations. For VOC removal cases, Mn catalysts have been found to be active in the two-stage process because of their high potential for utilizing  $\text{O}_3$ . However, Mn catalysts are less active when they are placed directly in the plasma zone (single-stage). This trend suggests that the optimum catalytic material for plasma catalysis can be found among hitherto less focused materials. More detailed discussion and future perspectives are discussed in Section 4.5.

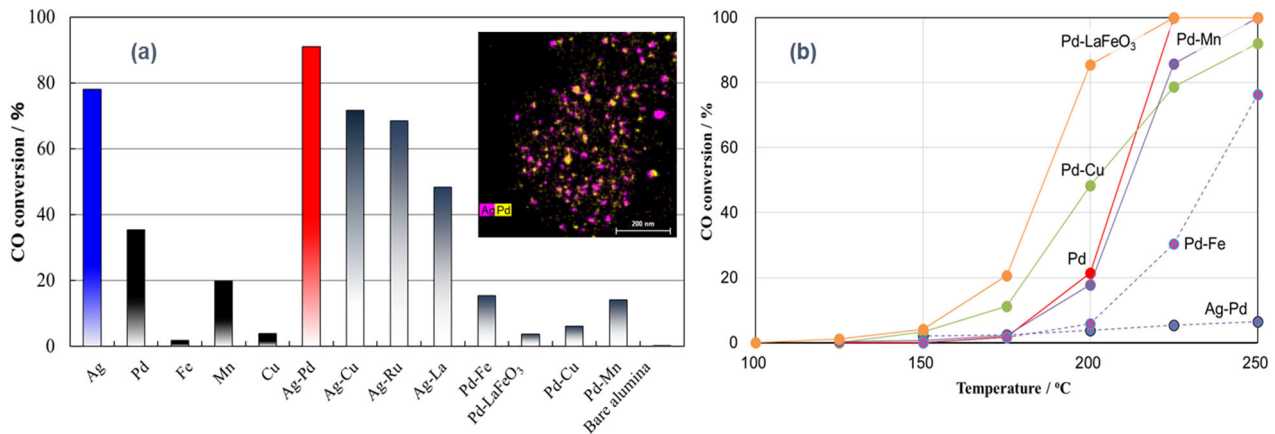


**Fig. 4.** Example of activity inversion for CO oxidation: (a) O<sub>3</sub>-assisted CO oxidation, (b) thermal oxidation of CO. The inset figure indicates HAADF-EDS of the Ag–Pd catalyst: [54] with permission from Elsevier.

## 2.2 Plasma-induced heating

One of the mandatory questions for plasma catalysis has been whether the reaction is solely driven by the heat provided from the plasma. In case of NTPs for environmental applications (PPM chemistry), plasma-induced gas heating ( $\Delta T$ ) has been neglected because it is generally operated with a relatively small SIE ( $\text{J L}^{-1}$ ). In the 1990s, plasma catalysis was intensively studied for treatment of exhaust gases from automobiles. At that time, the maximum SIE request from car manufacturers was approximately  $50 \text{ JL}^{-1}$ , which equals to about 3% of the fuel penalty. In laboratory-scale experiments focusing on fundamental aspects, less attention has been paid to energy consumption. However, careful attention to the energy input and the resulting heating is necessary to discriminate the working mechanism in plasma catalysis. In principle, a temperature increase can rearrange the properties of both the plasma and catalyst.

Fig. 5 shows the plasma-induced heating in the plasma reactor. The heating data of a plate-to-plate dielectric barrier discharge (DBD) reactor in air (1 mm gap) [56] and in He (3.1 mm gap) [57] is given as a reference (without packing materials). AIST data were measured with a fiber-optic thermometer, and Li *et al.* [58] used optical emission spectroscopy of the second positive system of N<sub>2</sub> to estimate the temporal gas temperature increase due to streamer propagation. The Eq. 3 line corresponds to the temperature increase, assuming that 100% of the discharge power is converted to temperature. However, as indicated in Eq. 4, heat loss occurs in the reactor, including the heat capacity of the packing material.

$$\Delta T = \left( \frac{P}{\rho_m c_p Q} \right) \quad (3)$$

$$\Delta T = \left( \frac{P}{\rho_m c_p Q} \right) - (\text{wall loss}) - (\Delta H) \quad (4)$$

Considering the intrinsic nature of plasma-induced heating, the real temperature of the catalyst bed ( $T_{\text{real}}$ ) will always be higher than the setting temperature ( $T_{\text{set}}$ ), as shown in Eq. 5. The two main factors for  $\Delta T$  are plasma-induced heating and the heat of reaction. The enthalpy change ( $\Delta H$ ) becomes negative for exothermal reactions and *vice versa* for an endothermic reaction.

$$T_{\text{real}} = T_{\text{set}} + \Delta T \quad (5)$$

In contrast to “PPM chemistry”, “PPH chemistry” usually requires a higher SIE value ( $> 1 \text{ kJ L}^{-1}$ ). In these cases, temperature control plays a pivotal role in the design and operation of any kind of catalytic process. Overheating induces the sintering of active metal components, which eventually leads to permanent deactivation. In the case of endothermic reactions, the temperature of the catalyst decreases as the chemical reaction initiates. Kameshima *et al.* visualized the temperature profiles of methane reforming reactions using infrared thermography [59].

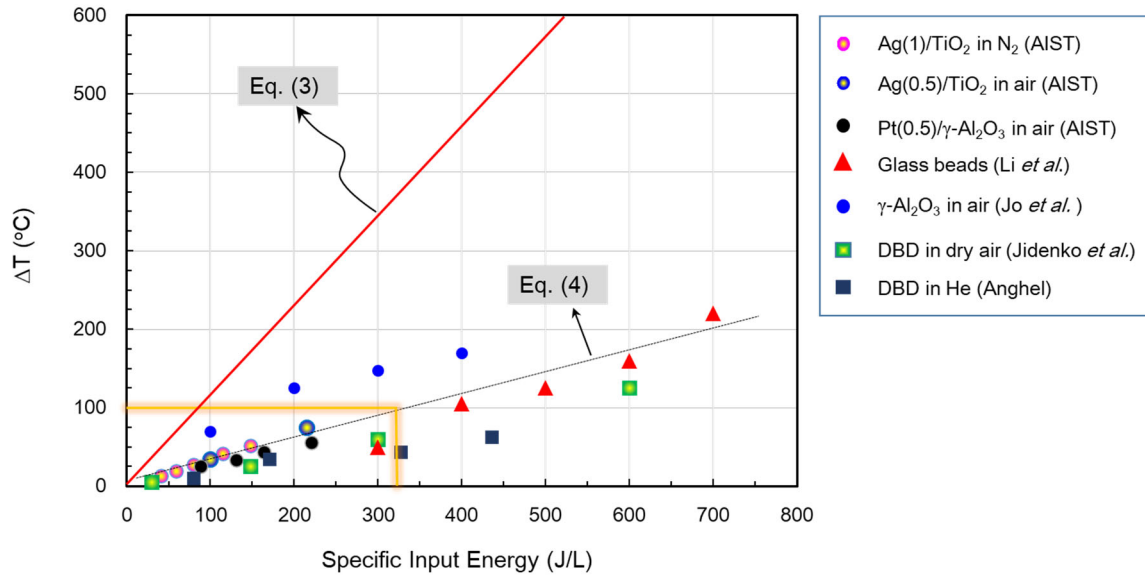


**Fig. 5.** Plasma-induced heating in a packed-bed with various materials. The Eq. (3) line indicates the gas heating trend assuming that all the input energy was used in gas heating.

The heat transfer characteristics in a two-parallel plate  $\text{CH}_4$ -fed DBD reactor were studied thoroughly based on energy balance, local gas heating effect, gas temperature measurement, and heat loss to the wall [60, 61]. When a streamer bridges the gas gap, the streamer further propagates along the dielectric barrier; therefore, 80% of the input power is lost to the wall as heat. Approximately 10% of the input power was used for the gas heating. This implies that, in the case of a packed-bed DBD reactor, the heat generated by streamers is transferred selectively to the catalyst pellets, as validated by high-speed imaging of streamer formation dynamics, showing that streamers propagate in close contact with the pellet surface and cover a wider surface area [62]. In the case of an endothermic reaction ( $\Delta H > 0$ : Eq. 4), the heat generated by the DBD is recovered efficiently as the enthalpy of the product species. Detailed gas temperature analysis was performed in a packed-bed DBD reactor for  $\text{CH}_4$  dry reforming using the rotational temperature of CO Ångström system [63]. As time- and space-averaged values, the gas temperature and catalyst bed temperature were equilibrated, and the temperature profile of the catalyst bed was visualized by infrared thermography. The plasma heating and energy efficiency are correlated with the SIE. For simplicity, stoichiometric  $\text{CH}_4$  dry reforming was assumed ( $\text{CH}_4 + \text{CO}_2 = 2\text{CO} + 2\text{H}_2$ ;  $\text{SER} = \Delta H = 247 \text{ kJ mol}^{-1}$ ). Here, SER represents the specific energy requirement. Considering the conservation of energy between the discharge power and endothermic reaction enthalpy, the following equation is obtained:

$$xF_{\text{CH}_4}\Delta H = \text{SIE} \times (F_{\text{CH}_4} + F_{\text{CO}_2}) = \text{SIE} \times F_{\text{CH}_4}(1 + \alpha) \quad (6)$$

$$\text{Energy efficiency} = \frac{x}{1+\alpha} \times \frac{\Delta H}{\text{SIE}} \quad (7)$$

$x$  denotes  $\text{CH}_4$  conversion ( $0 < x < 1$ ),  $F$  is the feed gas flow rate ( $\text{mol s}^{-1}$ ), and  $\alpha$  is the ratio of  $\text{CO}_2$  to  $\text{CH}_4$  flow rate. A similar definition is applicable to exothermic reaction systems [64]. When  $\text{SIE} = 123.5 \text{ kJ mol}^{-1}$  at  $\alpha = 1$  and  $x = 1$ , the energy efficiency becomes 100%. In other words, excess energy input beyond  $\text{SIE} = 123.5 \text{ kJ mol}^{-1}$  induces plasma heating and thermal reaction dominates the catalytic reaction; plasma-induced synergism is no longer anticipated with much lower energy efficiency. The SIE must be carefully tuned so that plasma heating is minimized, and the synergistic effect is maximized.

### 2.3 Definition of synergy

Over the last ten years, many studies have reported the synergy of plasma catalysis. However, in some cases, validation is obscure. This situation becomes distinct when a plasma catalysis reactor is operated with a high

SIE, which inevitably leads to the heating of the catalyst reactor to be reactive even without plasma. Synergy is one of the main issues in plasma catalysis. The lexicographic definition of synergy is that the combined effect is greater than the sum of their individual effects, as described in the following equation.

$$\text{Synergy Factor} = \frac{[\eta]_{\text{Plasma-Cat}}}{[\eta]_{\text{Plasma}} + [\eta]_{\text{Catalyst}}} \quad (8)$$

Here,  $[\eta]$  indicates the chemical conversion rate of either decomposition or synthesis. Subscripts indicate the type of reaction.

Fig. 6 shows three cases (a) – (c) of plasma catalysis in interpreting the obtained results. The key issue here is the heating effect in the presence of plasma. When the conversion with plasma catalysis exceeds the sum of each process ( $\text{SF} > 1$ ), i.e., case-(a) in Fig. 6, it can be considered as a synergistic effect exist. It is often considered that the catalyst temperature is identical with or without plasma. As indicated in the previous section, the plasma always induces heating according to the amount of injected energy. Temperature increase has also been confirmed in NTP jets, where it can even be touched with human skin [65]. Therefore, it is more reasonable to consider synergy, as in the case (b), where a slightly higher contribution of thermal catalysis and enhanced plasma-induced conversion are also considered. As indicated in Fig. 3 and Section 2.2, temperature is one of the available components from plasma; therefore, heating should be properly considered in process optimization. To properly address the synergy in plasma catalysis, it is important to avoid excess heating of the catalyst, where thermal catalysis becomes dominant over the other pathways. One important precaution is maintaining SIE below  $1 \text{ kJ L}^{-1}$  for considering synergy in plasma catalysis. For example, the discharge power of  $2 \text{ W}$  seems to be small, but it amounts to  $1.2 \text{ kJ L}^{-1}$  for a total flow rate of  $100 \text{ mL min}^{-1}$ . In the case of PPH chemistry, there are many papers mentioning synergy under SIE higher than  $1 \text{ kJ L}^{-1}$  and sometimes even  $> 50\text{--}250 \text{ kJ L}^{-1}$  at extreme conditions. In case (c) with a high SIE, the catalysts are thermally activated with sufficient activity to even cancel the synergy-like effect brought by the plasma. Careful consideration cannot be overemphasized to avoid controversy regarding synergy in plasma catalysis [31, 66, 67].

The main strategy to establish synergy for plasma catalysis is to maximize the contribution of plasma-induced species that have been wasted because of the lack of effective methods. Heating from the plasma can be effectively used to optimize the reaction. For example, a heat-tight reactor should be considered for the up-hill reaction, which requires heat to compensate for  $\Delta H$  by heat supply. Proper cooling may be necessary when plasma catalysis is applied for a downhill reaction with a large heat of reaction. Hot molecules of vibrationally or translationally excited states are considered rich seam for groundbreaking breakthroughs in plasma catalysis. The details are further discussed in Section 4.3.

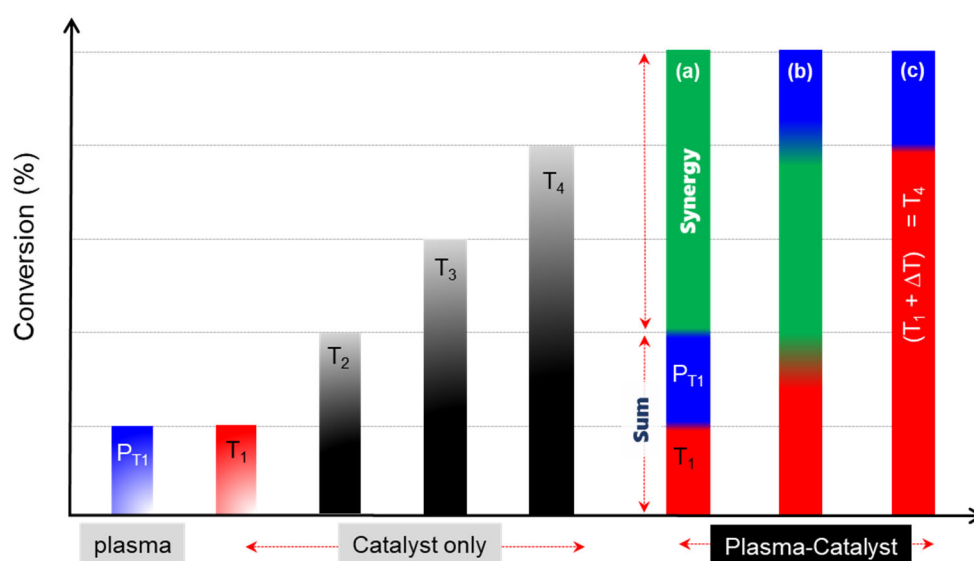


**Fig. 6.** Model cases of synergy in plasma catalysis.  $T_1$ – $T_4$  indicate the temperature in increasing order. Cases (a), (b), and (c) in plasma catalysis show the possible perspectives for understanding the synergy.

### 3. Recent developments

#### 3.1 Plasma catalysis reactors

##### 3.1.1 Packed-bed reactor and the effect of packing materials

The packed-bed type reactor was first developed for particle collection [68, 69], where ferroelectric materials ( $\text{BaTiO}_3$ ) were packed between two mesh electrodes. It has since been extended to sterilization [70], odor [71], and VOC removal [70, 72–74]. Packed-bed reactors with various packing materials have shortly become a platform device in plasma catalysis [75–77] owing to their simple structure and convenience. Fig. 7 schematically illustrates the packed-bed reactors developed in the 1990s. The most widely accepted effect of packing materials is electric field augmentation at the contact point between the pellets. Pellets can be considered as a series of capacitors and resistors. When a high voltage is applied to a packed-bed reactor, the voltage-drop simply follows the capacitance of the pellet ( $C_{\text{pellet}}$ ) and air gap ( $C_{\text{gap}}$ ). Since  $C_{\text{pellet}} \gg C_{\text{gap}}$  is established for most packing materials, partial discharge always initiates at the contact point when the electric field exceeds the breakdown voltage of the working gas. For materials with a high dielectric constant, such as  $\text{BaTiO}_3$ , partial discharge is always dominant over other discharge modes (see Fig. 7(a)). When proper catalysts are packed, surface streamers become dominant over the partial discharges, as shown in Fig. 7(c). The properties of packing materials that affect the discharge mode are surface conductivity [78], dielectric constant [77, 79], and size [80]. The catalysts packed in the plasma can directly interact with plasma, so the packed-bed reactor is often referred to as a single-stage, in-plasma, or plasma-driven catalyst reactor. There are also various types of reactors, including multi-stage reactors with different materials, but these are beyond the scope of this paper.

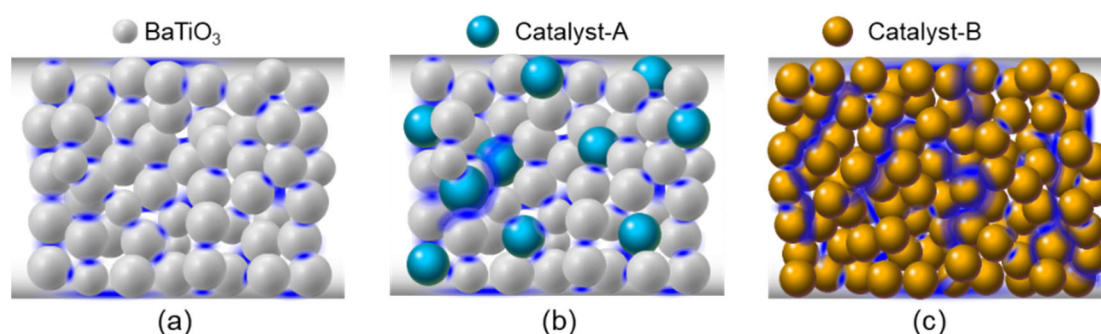


**Fig. 7.** Schematic of packed-bed reactors: (a) partial discharge only, (b) partial discharge dominant over streamer, (c) surface streamers dominant over partial discharge.

Packing materials can alter the plasma properties which leads to modification of chemical reactions to some degree. In the early 1920s, several studies on the packing a glass wool on electrical discharge were reported [81, 82]. Glass wool is generally considered to be inactive as a catalyst. However, the presence of glass wool alters the discharge more uniformly over the entire volume. Later, Gallon *et al.* observed plasma generation by intensified charge-coupled device (ICCD) imaging and confirmed the uniform discharge in the presence of glass wool [83]. Schmidt-Szalowski and Borucka investigated the effect of silica (1.2–3.2 mm) packing on ozone generation. They reported that silica packing increased ozone concentration by 1.4 to 1.6 times with higher ozone yield [84]. However, the observed packing effect can be explained by the modification of the plasma distribution in space, which has less to do with catalytic action.

After 2000, unsupported materials, such as  $\gamma\text{-Al}_2\text{O}_3$ , and zeolite, were tested and found to be effective when used alone or in combination with  $\text{BaTiO}_3$ . For example,  $\gamma\text{-Al}_2\text{O}_3$  has a relatively large surface area ( $\sim 300 \text{ m}^2 \text{ g}^{-1}$ ), so it can trap large numbers of molecules on its surface, including in its inner pores. In the case of pollutant removal (PPM chemistry), packing materials with high surface areas significantly alter the reaction conditions from “large volume with low concentration” to “small area with high concentration” [85–87]. Six plasma-induced particles can effectively collide with molecules concentrated on the surfaces, which can lead to an increase in energy efficiency. This adsorption-induced modification of concentration and space may play a role in PPM chemistry, but it is a less important form of chemistry.

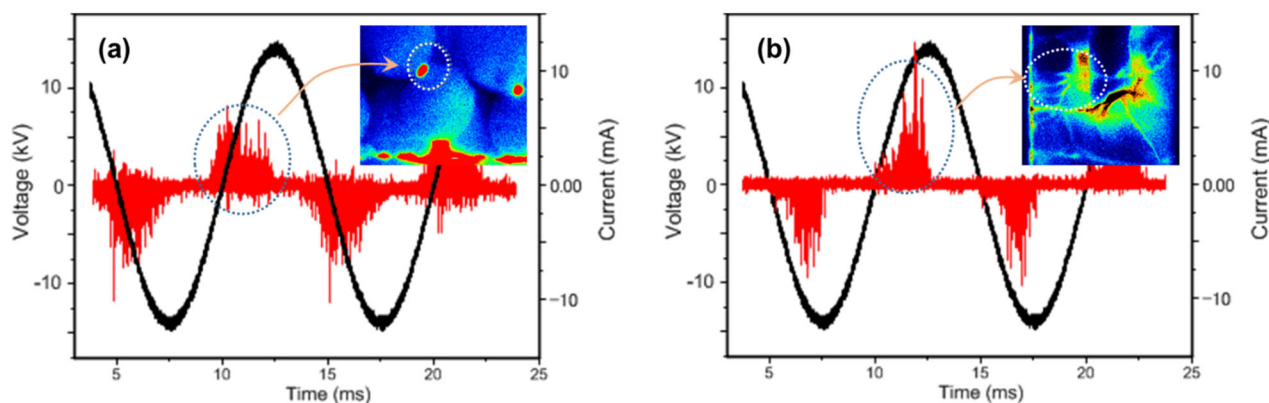


**Fig. 8.** I-V characteristics and discharge pattern with (a) BaTiO<sub>3</sub> ( $\epsilon_s = 10000$ ), (b) Ag(10)/HSY. Inset ICCD camera photos are taken under discharge in air. Reproduced with permission from the Institute of Electrostatics Japan (IPEST).

Fig. 8. shows voltage-current waveforms for (a) BaTiO<sub>3</sub> and (b) Ag/HSY catalysts [88]. There is no apparent difference between the BaTiO<sub>3</sub> beads and the Ag/HSY pellets. In both cases, the plasma consisted of a number of current pulses that resemble each other. Each current pulse had a full width at half maximum (FWHM) of approximately 40 ns. Similar I-V characteristics do not assure a similar plasma pattern, especially in the catalyst-packed plasma reactor. Considering the small plasma area in the case of BaTiO<sub>3</sub> beads, relatively dense plasma is produced in a fixed area (at the contact points of pellets), which may result in high plasma density. This dense current flow in a small volume may increase the gas temperature. This temperature effect was experimentally confirmed by the low ozone formation and high NO<sub>x</sub> formation in the case of a BaTiO<sub>3</sub>-packed reactor [89].

From the perspective of effective surfaces involving chemical reactions, pellets have a structural disadvantage over honeycomb. The large pressure drop in a packed-bed reactor is another important drawback. At present, packed-bed reactors can still be useful for laboratory-scale studies to measure the effect of various parameters.

### 3.1.2 Honeycomb discharge

Honeycombs are of great importance in heterogeneous catalysis, as they provide a high surface-to-volume ratio, low pressure drop, and high mass and heat transfer. A combination of plasma and honeycomb catalysts can be performed either in a two-stage system [90] or a one-stage system depending on the position of the honeycomb catalyst [8, 91]. The generation of stable discharges through the channels of the honeycomb represents a major challenge in honeycomb discharge from a practical perspective. The discharge in such a confined geometry of channels has a relatively high onset voltage compared to the discharge generated in open (non-confined) air, due to the loss of charged particles by interaction with the channel walls. This discharge is often less stable with frequent sparking, which can eventually lead to undesired mechanical damage to the ceramic channel walls. Moreover, it is also difficult to achieve uniform plasma distribution inside honeycomb channels when using adequate discharge power. Nevertheless, in recent years, progress has been made in honeycomb discharge both experimentally (for both multiple capillaries and honeycomb monoliths) and theoretically [92, 93].

The first studies on plasma combined with honeycomb catalysts (honeycomb monoliths and bundles of capillaries) in a common system appeared approximately 20 years ago. Fundamental studies have mostly used transparent capillaries suitable for visualization and optical emission spectroscopy. For example, Blin-Simiand *et al.* visualized the discharge propagation inside honeycomb channels using an ICCD and found plasma filaments randomly distributed inside honeycomb propagating both along and across the channels [94]. The reactor design considered in the last ten years includes wire-to-ground (Fig. 9a, b) [95–98], wires-to-wires (Fig. 9b, c) [99, 100], mesh-to-mesh vertical (Fig. 9d) [91, 101–103] or parallel to honeycomb [99], pin-to-mesh (Fig. 9e) [104], plane-to-plane (Fig. 9f) [94], sliding discharges (AC discharge with an additional DC electrode) coupled with a packed-bed reactor (Fig. 9g) [2, 105–109], sliding discharge with surface discharge (Fig. 9h) [2, 108, 110], and sliding discharges with micro-hollow surface DBD (Fig. 9i) [2, 110], two micro-hollow

surface DBD between a honeycomb monolith (Fig. 9j) [108]. The materials considered for honeycomb are cordierite [91, 94, 100, 102, 103], Cu/ZSM-5 [98], HZ-B zeolite [96, 97], and diesel particulate filter (DPF) [104, 111].

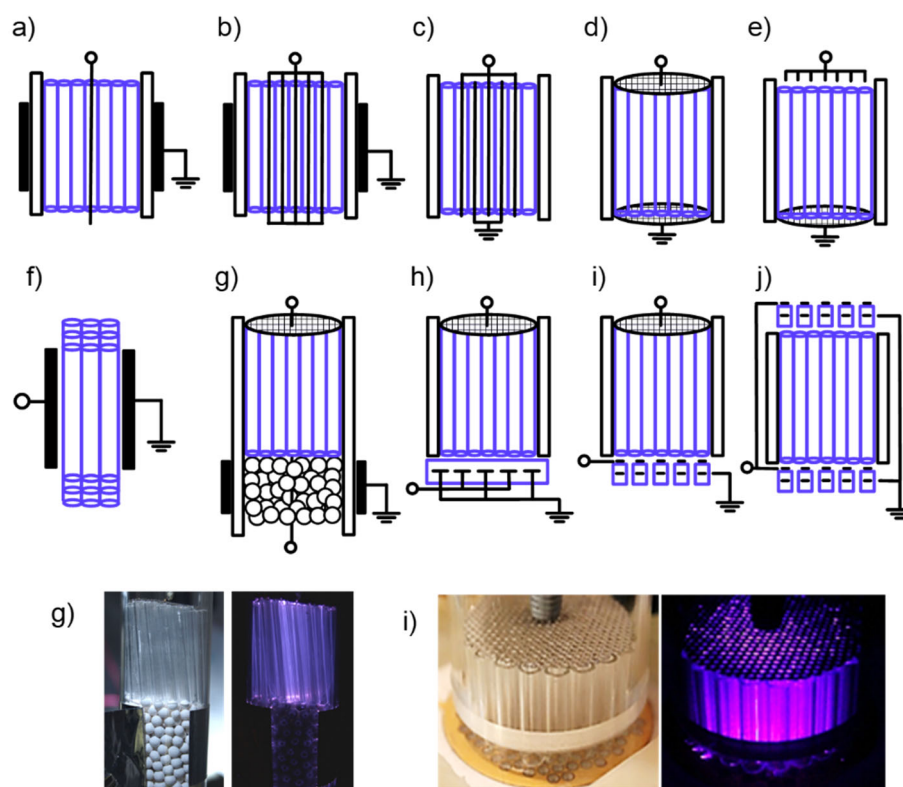


**Fig. 9.** Various geometries and electrode configurations for honeycomb discharge generation.

In addition to experimental works, several studies have been conducted on numerical simulations of plasma generation and propagation inside honeycomb monoliths or similar geometries. Jansky *et al.* simulated discharge propagation in capillary tubes of a honeycomb catalyst and studied the effect of tube radius and permittivity on the discharge structure and its propagation velocity [92, 93]. They reported an increase in discharge velocity and change in its tubular structure to homogeneity with diminishing radius as a result of the change in the electrical field distribution. In contrast, Zhang *et al.* simulated the discharge propagation in honeycomb and studied the interaction of plasma with the capillary tube material [112]. The simulations showed that the discharge velocity was enhanced when the discharges were initiated at the dielectric surface rather than at the center of the capillary tube owing to the surface charging process. This process creates an additional electric field along the surface, enhances the electron density, and increases the discharge propagation velocity.

The systems were studied for both their physical and chemical properties. Hensel *et al.* investigated the effect of the diameter and length of capillary tubes on the electrical and optical characteristics of discharges [106, 107, 113]. Takashima *et al.* studied the effects of air humidity and temperature on honeycomb discharge generation and properties and found a positive effect on the discharge stability [108]. Cimerman *et al.* showed that discharge stability, as well as light emission intensity, is supported by an increase in both the air flow rate and air relative humidity [110]. The chemical activity of the discharges was tested in terms of ozone production [110], NO<sub>x</sub> removal in the selective catalytic reduction (SCR) using an Fe-zeolite-supported honeycomb catalyst [109], and the regeneration of diesel particulate [111].

Recently, Mok and co-workers introduced a large humidified air plasma using a sandwich-type honeycomb plasma (SHP) configuration, as shown in Fig. 10 (a), and (b) [91]. The SHP reactor is comprised of two mesh/perforated electrodes acting as a high-voltage and ground electrode and honeycomb catalyst located inside the two electrodes with an adjustable distance between the electrode and honeycomb side. They also examined the dependence of honeycomb plasma discharge (HPD) on reactor configuration, honeycomb

composition, and temperature to reveal plasma discharge by an SHP [91, 102, 114]; an initial application for environmental issues was also performed [103]. As shown in Fig 10 (b), the discharge power increased significantly with the water content in the gas mixture [91]. Under proper conditions, the plasma discharge developed inside the channels of the monolith as shown in Fig. 10 (d). One reason for the plasma development in the honeycomb channel is the enhancement of the relative permittivity ( $\epsilon$ , dielectric constant) of the monolith with water vapor [114]. Another important factor is the surface conductivity, which is clearly seen by the sharp decrease in impedance with an increase in water vapor. A similar conclusion was published for DBD microdischarges in humid air mixtures [115]. Takashima *et al.* reported a positive influence of higher humidity in capillary honeycomb discharges in terms of stability and extension of the plasma area [108].

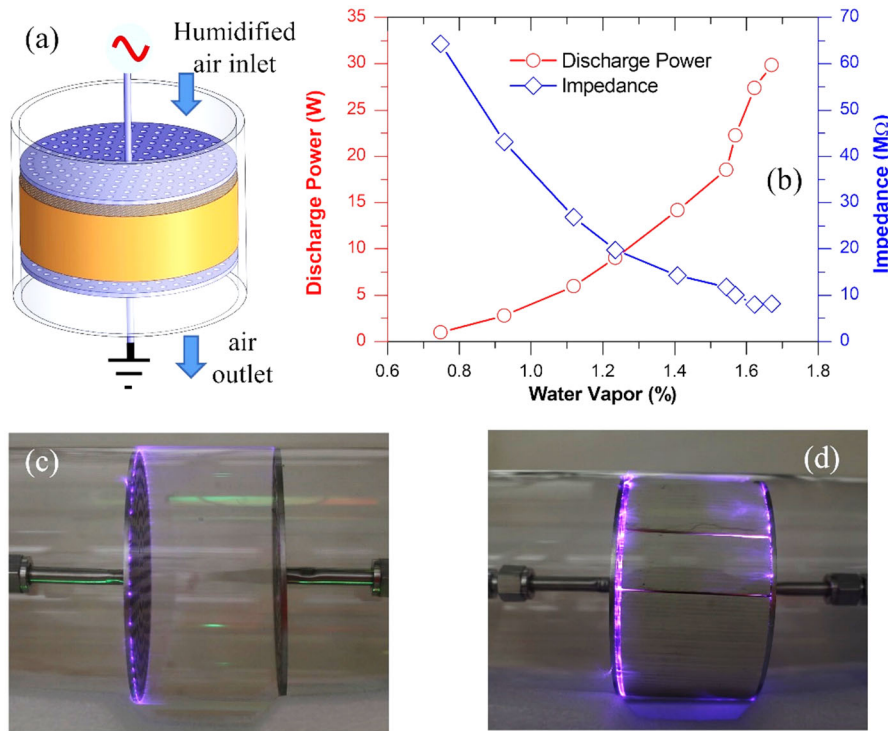


**Fig. 10.** (a) Honeycomb reactor. (b) Effect of water vapor content in the discharge power and impedance (bare monolith; total flow rate: 75 L min<sup>-1</sup>, applied voltage: 25 kV), data adapted from [91]. Images of plasma discharge (c) without monolith and (d) with bare monolith (total flow rate: 60 L min<sup>-1</sup>, 30 kV, 50 mm in honeycomb thickness, 93 mm in diameter, 300 cups,  $d_h = 2$  mm,  $d_g = 0$  mm), (c) and (d) reprinted from [114] with permission from IOP Publishing.

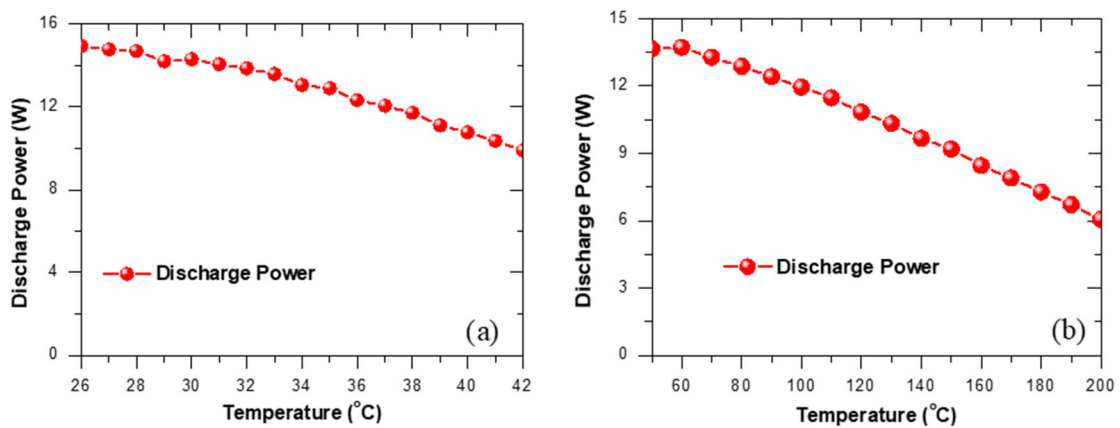


**Fig. 11.** (a) Dependence of discharge power on (a) ambient condition variation (30 kV; % H<sub>2</sub>O: 2.3%; flow rate: 60 L min<sup>-1</sup>; monolith diameter: 93 mm; temperature increase: 1 °C min<sup>-1</sup> bare monolith) and (b) high temperature variation (applied voltage: 25 kV; % H<sub>2</sub>O: 3%; flow rate: 25 L/min; monolith diameter: 30 mm; temperature increase: 5 °C min<sup>-1</sup>; metal coated-commercial monolith). (a) was adapted from [114] with permission from IOP Publishing.

The performance of the HPD was found to be highly dependent on the applied voltage, flow rate, electrode configuration, distance, monolith type and temperature. Fig. 11 shows the effect of the temperature on the discharge power. The temperature increase from 26 to 42 °C reduced the discharge power from 15 to 10 W, that is a reduction in discharge power of  $\sim 0.3\text{W}/^\circ\text{C}$ . A similar trend was observed at higher temperatures (b). Simultaneously, the performance of the HPD decreased with temperature. It is postulated that the modification of electrical components (i.e., surface conductivity, and capacitance) by the adsorbed water on the monolith is the main reason, but this needs to be studied in detail.

This section gives a brief historical review of the development from capillary discharges to honeycomb discharges. Although there are still issues to be resolved and improved, honeycomb discharge will play an important role in practical applications. One such issue is that the total volume of plasma is often unknown, and it is not clear whether it is generated in every channel of the honeycomb catalyst. Another issue is the stability of the discharge and its mode (streamer, spark) which is critical for applications, such as exhaust gas cleaning and DPF regeneration. As indicated in Section 2.1.5, a tailored design of honeycomb materials is required for the best matching with plasma. Nevertheless, systems of honeycomb discharge have shown great potential and many of the presented works may serve as a good starting point for future experimental investigations at larger scales.

### 3.1.3 Fluidized-bed DBD reactor

Unlike thermal catalysis, improving the mutual interaction between NTP and a catalyst (five matching) requires a peculiar strategy because plasma is neither generated nor diffused into micropores (Section 2.1.3). A packed-bed DBD (PB-DBD) is a form of fixed-bed reactor characterized as "random packing" configuration. A honeycomb-type fixed-bed reactor is characterized as "structured packing" [116]. The honeycomb reactor is commonly used for exhaust gas treatment of automobiles, as discussed in Section 3.1.2, and the contact area between the gas and honeycomb is maximized with a minimum pressure drop.

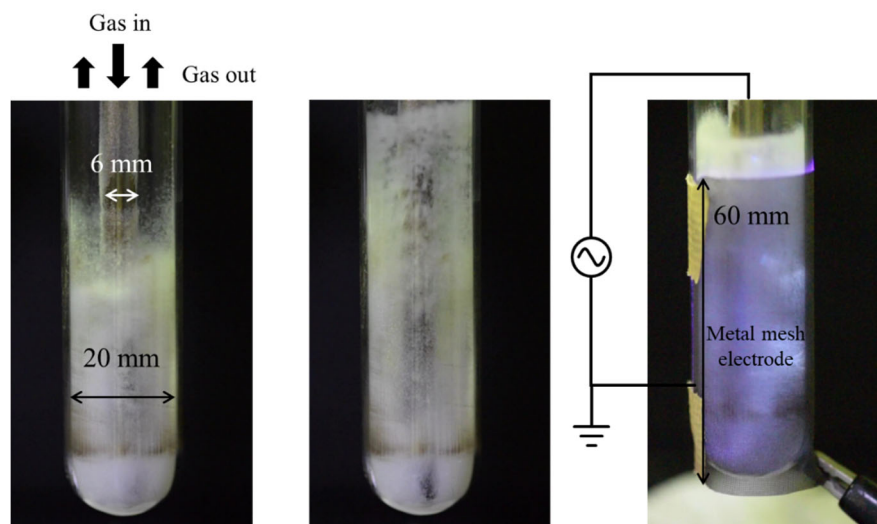


**Fig. 12.** Fluidized-bed DBD reactor.  $\text{SiO}_2$  (300-425  $\mu\text{m}$ ), 4 g loaded,  $\text{CO}_2$ :  $200\text{ cm}^3\text{ min}^{-1}$ , 2.5 Pa, 25 °C, 30 W (12 kHz sinusoidal high voltage).

Meanwhile, the PB-DBD is easy to construct and has become a standard configuration in laboratory-scale experiments. A fluidized-bed reactor is well known for its excellent heat and mass transport performance; thus, a high interaction between the plasma and catalyst is anticipated. However, due to the difficulty in ensuring a better fluidized motion of the catalyst powder, a limited number of studies are available. Sekiguchi *et al.* studied a spouted-bed reactor combined with gliding arc discharge for  $\text{CH}_4$  reforming with Ar dilution [117]. Crushed  $\text{Al}_2\text{O}_3$ -supported catalysts containing different metals were studied (Ru, Rh, Pt, and Pd).  $\text{CH}_4$  conversion was unexpectedly low because the temperature of the gliding arc was estimated to be below 300 °C, and the reactor temperature was lower than 100 °C. Therefore, catalyst-dependent reactivity and plasma-induced synergism were not confirmed. In addition, the electrical properties of the spouted-bed gliding arc discharge were not presented. Wang *et al.* has studied  $\text{CH}_4/\text{CO}_2$  reforming with Ar dilution using a fluidized-

bed DBD (FB-DBD) reactor and compared its performance with that of a PB-DBD reactor [118]. Crushed Ni/Al<sub>2</sub>O<sub>3</sub> catalysts with meshes from 70 to 100 were used (power size ranged from 210 μm to 150 μm) and SIE ranged from 0.20 to 0.79 eV molecule<sup>-1</sup>. The fluidized motion of the catalyst powder was not presented, and the CH<sub>4</sub> and CO<sub>2</sub> conversions of the FB-DBD were poorer than those of the PB-DBD. The authors calculated the degree of synergy using the same definition as in Eq. (8): the synergy factor for CH<sub>4</sub> conversion is 1–1.25 with no difference between the FB- and PB-DBD reactors. Note that a synergy factor = 1 indicates that there is no synergistic effect of DBD. As for CO<sub>2</sub> conversion, that of the FB-DBD was slightly higher than that of the PB-DBD; the reverse water gas shift (RWGS) reaction (CO<sub>2</sub> + H<sub>2</sub> = CO + H<sub>2</sub>O) was promoted by the DBD, yielding a smaller amount of H<sub>2</sub>. More recently, Bouchoul *et al.* have studied an FB-DBD reactor for CH<sub>4</sub>/CO<sub>2</sub> reforming with 75 vol% He dilution (SIE = 1.52 eV molecule<sup>-1</sup>) [119]. Al<sub>2</sub>O<sub>3</sub> grains with sizes of 355–650 μm were used. Similar to Ref [118], the reforming performance of the FB-DBD was poorer than that of the PB-DBD. In Ref. [117, 119], fluidized behavior was not provided by either images or movies; therefore, detailed heat and mass transport capability was difficult to analyze. Moreover, Ar or He was used for the large dilution. In all cases, the reforming performance was poorer than that of the PB-DBD reactor. Nozaki *et al.* successfully developed an FB-DBD reactor that operated at 5–20 kPa and 20–400 °C without dilution gas. Fig. 12 shows a snapshot of the FB-DBD using 4 g SiO<sub>2</sub> powder (300–425 μm). CH<sub>4</sub>/CO<sub>2</sub> reforming and CO<sub>2</sub> hydrogenation have been investigated using various types of catalysts (SIE < 1.5 eV molecule<sup>-1</sup>). The reforming performance of FB-DBD was clearly enhanced by PB-DBD in all cases. The results will be published shortly.

### 3.2 Catalyst regeneration and industrial use

Plasma catalysis includes the application and implication of discharge phenomena in the overall life of catalysis or preparation, reaction, and even regeneration of the catalyst. The catalyst can provide the benefit of reducing the activation energy barrier. However, because the catalytic function is based on the surface chemistry of the active sites of a catalyst, there could be physical and chemical changes in the surface during the course of the reaction that could deteriorate the chemical function of the catalyst. The deactivation of the catalyst has diverse mechanism depending on the origin of the deactivation. The aspects of deactivation can be classified into 1) carbon deposition, 2) oxidation, 3) sintering, 4) poisoning, 5) fouling. These aspects of deactivation are tabulated below [120].

Some of the above types of deactivation can be resolved by removing the reasons for deactivation and restoring the active sites. However, other types of deactivation, such as sintering and physical fracture of microstructures cannot be regenerated. The main methods of achieving regeneration are 1) thermal regeneration, where high-temperature conditions can remove impurities and fouling, and 2) supplying chemical species that can react with impurities, resulting in the removal of such impurities. Here, plasma can

Table 1. Mechanisms of catalyst deactivation [120].

| Mechanism                             | Type                      | Brief definition/description   |
|---------------------------------------|---------------------------|--|
| Poisoning                             | Chemical                  | Blockage of catalytic sites by strong chemisorption of some species  |
| Thermal degradation and sintering     | Thermal or thermochemical | Thermally induced loss of catalytic surface area, support area, and active phase-support reactions                   |
| Fouling                               | Mechanical                | Physical deposition of species from the fluid phase onto the catalytic surface and in catalyst pores                 |
| Vapor formation                       | Chemical                  | Production of volatiles in the reaction of gases with the catalyst phase   |
| Vapor-solid and solid-solid reactions | Chemical                  | Reaction of vapor, support, or promotor with the catalytic phase to produce an inactive phase                        |
| Attrition/crushing                    | Mechanical                | Loss of catalytic material due to abrasion; loss of internal surface area due to mechanical crushing of the catalyst |

play a role in the regeneration of the deactivated catalyst. Plasma can supply heat either directly or indirectly (plasma-assisted combustion). Plasma can supply species such as reactive oxidants (O, O<sub>3</sub>, OH) or reductants (H, H<sub>2</sub>). The followings are representative cases of catalyst regeneration using plasma. First, the plasma itself can provide heat for the catalyst. However, heating by plasma alone can raise the issue of energy cost. A plasma burner that can supply a strong flame stabilization mechanism can be an effective tool for heating with minimized use of electric power by utilizing the chemical energy of fuel released by combustion. Removal of ammonium bisulfate (ABS) by a plasma burner is a good example of such an application [120]. The temperature of the exhaust gas after the turbocharger in a low-speed marine engine is approximately 200 °C. Because of low-temperature conditions in the SCR reaction and sulfur content in the fuel, ABS is generated, and the catalyst becomes deactivated by fouling of ABS (see Fig. 13 left). A plasma burner can be used for the regeneration of ABS by heating the catalyst above 350 °C. Fig.13 shows a catalyst before and after catalyst regeneration, with a plasma burner used as a heat source [120].

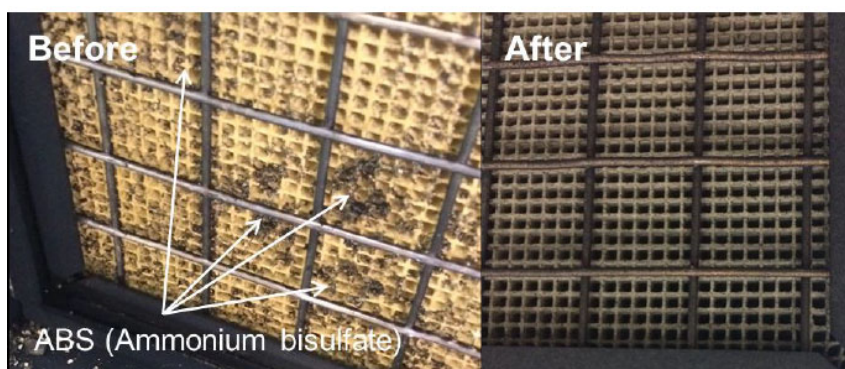


**Fig. 13.** Deactivated SCR catalyst by ABS fouling (left) and the same catalyst after regeneration (right). With permission from Elsevier.

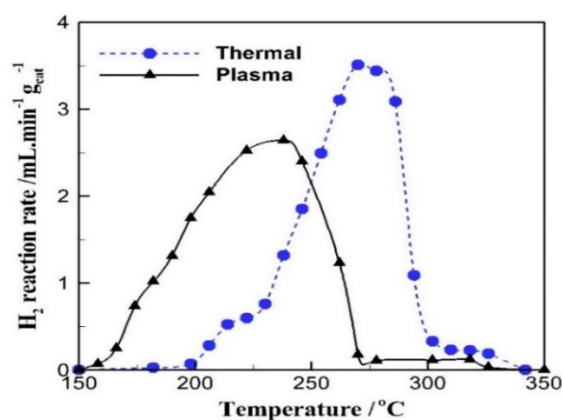


**Fig. 14.** H<sub>2</sub> temperature-programmed reduction (TPR) patterns that compares plasma and thermal reduction of CuO to Cu [122]. With permission from Springer.

Second, plasma can play an important role in the desorption and oxidation of the deposited material in the catalyst. Ozone injection and oxygen plasma can be used for the removal of accumulated carbon on the packed reactor with an Au/TiO<sub>2</sub> catalyst, where discharge in the catalyst bed produces enhanced desorption and removal of carbonaceous deposits [121]. Plasma can also be used to reduce oxidized metal catalysts. Plasma can provide different reaction paths with the help of plasma-generated H radicals that can induce an Eley-Rideal type reaction with oxygen in CuO. The H radical-initiated reaction path can remove the rate determining-step (desorption of water from the catalyst) of reduction by desorption of the excited surface OH. Removal of the rate-determining step results in an enhanced reduction performance or reduction in lower temperature conditions than that of thermal regeneration. Fig.14 shows a comparison of the plasma reduction and thermal reduction of the CuO catalyst to Cu.

A specific feature of chemical regeneration of the catalyst by plasma is that the beginning of regeneration may originate not from surface-adsorbed species but from plasma-generated gas phase species (radical or excited molecules) before adsorption. This difference can result in differences in the kinetic of the reaction and

different surface energies. One aspect to consider in the regeneration of catalysts in plasma catalysis is that the discharge itself can vary with the progress of catalyst regeneration. During regeneration, the catalytic surface experiences a change in conductivity and dielectricity, which affects the discharge itself. Therefore, in the course of designing the reaction conditions for the regeneration of a catalyst, this type of possible change should be considered.

### 3.2.1 Cases of commercial-level technology: DPF regeneration

Together with  $\text{NO}_x$ , particulate matter (PM) is a representative emission of diesel engines. PM is a type of agglomerated carbon or carbonaceous organic material. DPF is the most widely adopted technology for PM removal. PM is deposited on the filter and should be regenerated or burned out periodically. To elevate the exhaust gas temperature above  $550\text{ }^\circ\text{C}$ , which is required to burn out the accumulated PM, a heat source is required. A plasma burner can provide a wide flammability and stable flame in oxygen deficient and rapidly varying flow rates of exhaust gas [123]. The plasma DPF system has been applied in heavy-duty trucks in the air force of Korea. Fig. 15 shows the removal efficiency of PM in 39 military trucks measured using an opacimeter. For the 39 tested vehicles over a three-year testing period, 98 % of average PM removal and successive regeneration of DPF were achieved by the plasma burner.

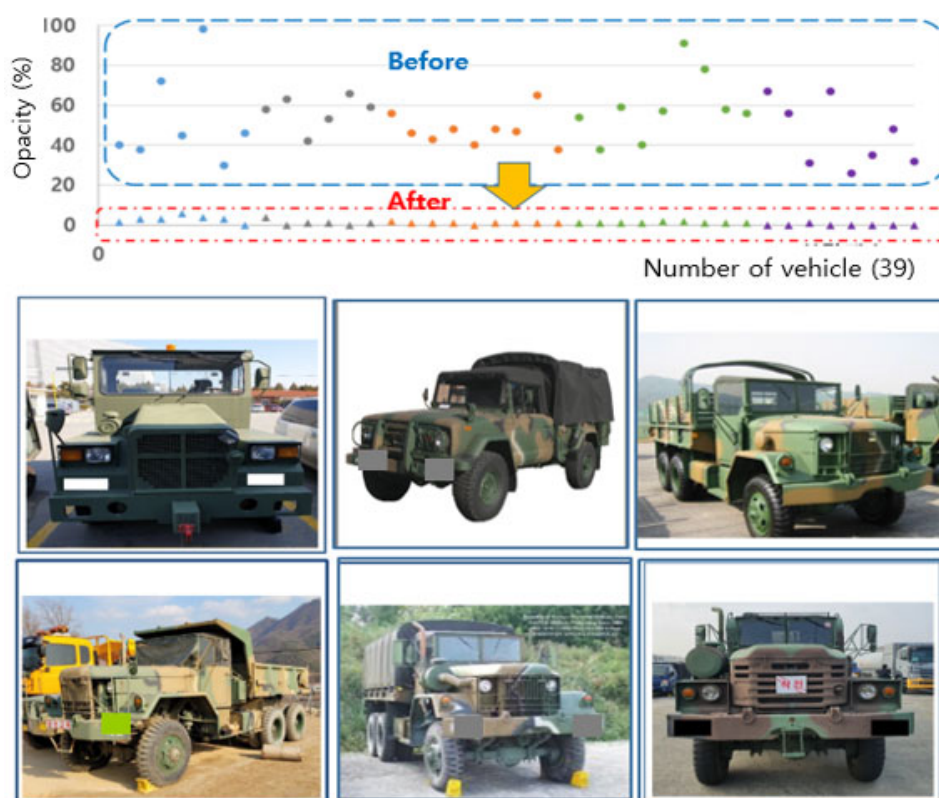
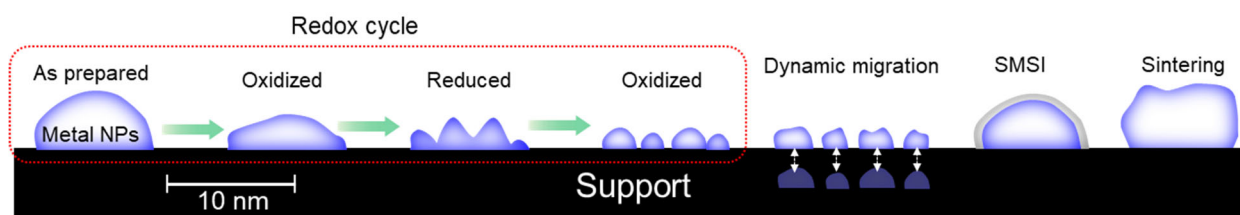


Fig. 15. Removal performance of PM in diesel truck operated by plasma DPF technology.

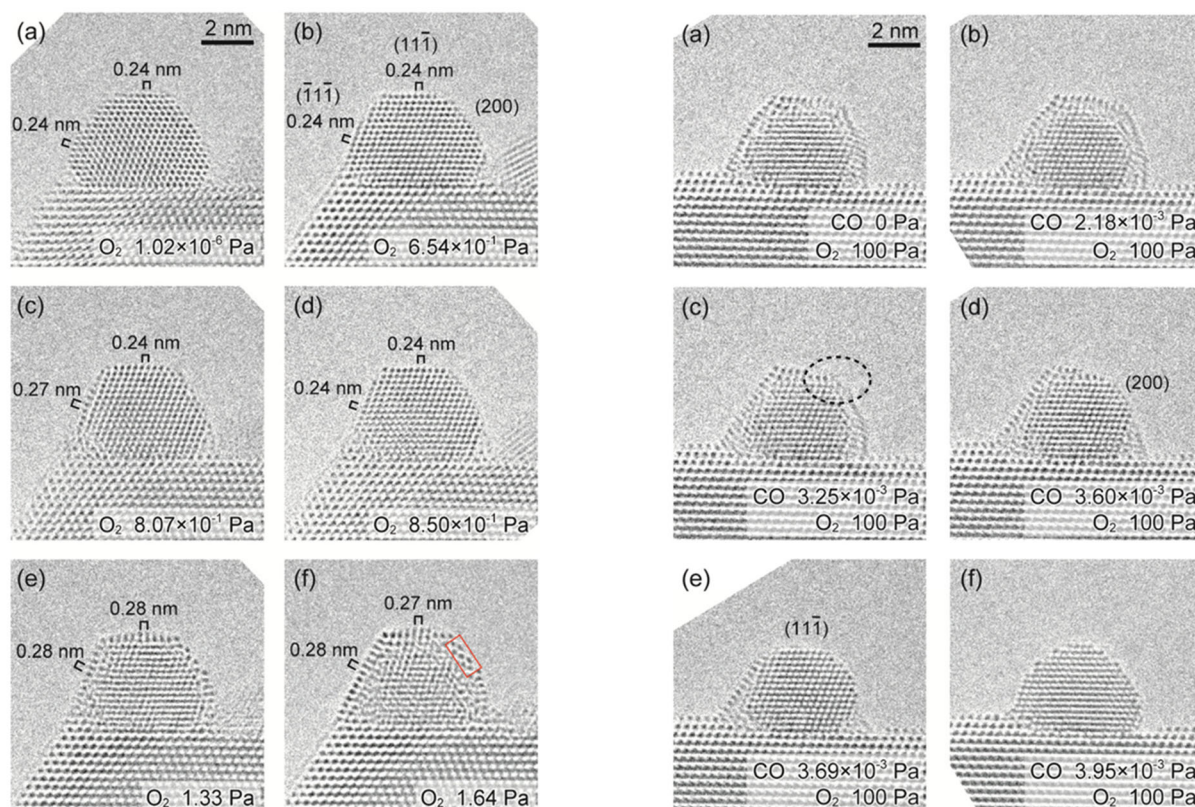
## 4. Future challenges

### 4.1 Surface dynamics of supported nanoparticles

The surfaces of metal NPs constitute active sites for most catalysts. A primary concern in catalyst preparation is the uniform distribution of small supported metal NPs to maximize the surface area. A variety of methods of decorating metal NPs on the surface of a support with small size and high dispersion have been developed. The prepared metal NPs are often subjected to dynamic changes according to the sequential processes of adsorption, reaction, and desorption. Fig. 16 schematically describes the reconstruction of the metal NPs along with the reaction conditions. Early evidence on the surface reconstruction of Rh and Pt–Rh alloy particles was



(A) Dynamic reconstruction of metal nanoparticles

(B) Oxidation of Pt/CeO<sub>2</sub> in O<sub>2</sub>(C) Reduction of Pt/CeO<sub>2</sub> in CO/O<sub>2</sub>

**Fig. 16.** Dynamics of supported NPs during redox cycles; (A) dynamic reconstruction of metal NPs, (B) environmental TEM (ETEM) images of atomic scale Pt oxidation in O<sub>2</sub>, (C) reduction of Pt oxide in CO/O<sub>2</sub>. The time scale of reduction from (a) to (f) was approximately 600 s. (B) and (C) reproduced by permission of The Royal Society of Chemistry (RSC) [132].

reported by Wang and Schmidt using transmission electron microscopy (TEM) [124]. The size and morphology of the Pt–Rh NPs changed when they were exposed to the redox cycle. A similar observation was also reported for a Co catalyst for the Fischer–Tropsch reaction [125]. Balcerzak *et al.* [126] observed reversible peak shifts of Ru ( $\text{Ru}^0 \rightarrow \text{Ru}^{2+} \rightarrow \text{Ru}^0$ ) in various redox environments using *in situ* X-ray photoelectron spectroscopy (XPS) analysis. Strong metal-support interaction (SMSI) is an interesting phenomenon in which the supported metal NPs are covered by a thin layer of support after exposure to high temperature. The SMSI is usually observed with supports such as TiO<sub>2</sub> and CeO<sub>2</sub>, but not for SiO<sub>2</sub>. Interestingly, the effect of the SMSI depends on the type of reaction. For most environmental applications, such as exhaust gas cleaning in automobiles and CO removal in air, the SMSI is detrimental to catalytic performance [127]. When a metal NP is completely encapsulated, it is in a state often referred to as the catalyst passive state or simply the SMSI state. However, it benefits from the Fischer–Tropsch process because highly active interfaces are formed between the Ru NPs and TiO<sub>2</sub> [128]. Bonanni *et al.* demonstrated that Ar ion sputtering and subsequent annealing at 1100 K can transform fully passivated Pt/TiO<sub>2</sub> catalyst (i.e., SMSI state) to a highly active form [127]. Sintering is a well-known mechanism that leads to the permanent deactivation of the catalyst. Two proposed mechanisms, particle migration and coalescence (PMC) and Ostwald ripening (OR), are also related to the surface dynamics of metal NPs [129, 130]. In the case of Pt/Al<sub>2</sub>O<sub>3</sub> at 600 °C, small Pt NPs (~ 5

nm) migrated at  $270 \text{ nm h}^{-1}$ , but larger particles ( $\sim 24 \text{ nm}$ ) moved at a distance equal to their diameter. The loss of small NPs is correlated with a rapid decrease in catalytic activity. Proper matching between the active metal and the support can mitigate the deactivation process. Nishihata *et al.* [131] indicated that Pd NPs can reversibly move into and out of the perovskite lattice and demonstrate long-term stability.

The advent of operando measurement techniques provided an important insight into the nature of supported NP catalysts, which are usually considered as active sites for surface reactions. An important tool is environmental transmission electron microscopy (ETEM), which can measure samples under realistic reaction gas mixtures. Yoshida *et al.* [132] measured Pt NPs with varying gas partial pressures of CO and O<sub>2</sub>. Fig. 16 (B) shows the oxidation progress of Pt with increasing O<sub>2</sub> partial pressure (up to 1.64 Pa) at room temperature. The initial Pt(111), (a), showed an atomic distance of 0.24 nm and surface reconstruction gradually appeared with increasing O<sub>2</sub> partial pressure to  $8.07 \times 10^{-1} \text{ Pa}$ , finally reaching atomic distances of 0.27–0.28 nm, which were assigned to  $\alpha$ -PtO<sub>2</sub> and  $\beta$ -PtO<sub>2</sub>. Under the tested conditions, oxidation of Pt NPs occurred only in several atomic layers from the surface. The PtO<sub>2</sub> particles can be reduced, as shown in Fig. 16 (C), by adding CO, which is six orders of magnitude smaller than O<sub>2</sub>. As the CO partial pressure was increased to  $3.25 \times 10^{-3} \text{ Pa}$ , the top right corner (circled area) began to decrease. Finally, the Pt oxides were completely reduced to metallic Pt at a CO pressure of  $3.95 \times 10^{-3} \text{ Pa}$ . Interestingly, the reduced Pt showed round edge and facet indexes, (110) and (311), which were also different from the original stage (111). This operando analysis clearly demonstrates that the supported Pt NPs undergo dynamic changes according to the reaction conditions. They also reported similar dynamics of Au-AgO nanofacets in a CO/air mixture [133] and Au/CeO<sub>2</sub> in CO/air [134].

Plasma can provide both highly oxidative and reductive environments on the surface of the catalyst. Several groups experimentally observed the size changes of supported metal NPs before and after plasma catalysis. For example, Jwa *et al.* [135] used a Ni/ $\beta$ -zeolite catalyst for the methanation of CO/CO<sub>2</sub>. TEM images and X-ray diffraction (XRD) patterns indicated that Ni particles were reduced from 25.8 nm to 18.7 nm with better dispersion. Understanding the dynamic changes of metal NPs may provide adequate evidence for “whys” and “why nots” in plasma catalysis.

Catalyst preparation using plasma is also highly linked with the dynamic behaviors of metal NPs at the nano- and atomic scales [136]. Plasmas can treat catalysts for calcination, oxidation, and reduction at much lower temperatures [137]. Low-temperature processing is attractive for metal NPs that are susceptible to agglomeration at high temperatures. A variety of plasmas have been used instead of thermal calcination: O<sub>2</sub> plasma [138, 139], H<sub>2</sub> plasma [140], Ar plasma [141], RF plasma [142], glow discharge [143, 144],  $\gamma$ -ray irradiation [145], and O<sub>3</sub> injection [146]. There have been several reports on the substantial changes in supported metal NPs after exposure to plasma.

Table 2 summarizes the reported plasma effects on the catalysts. Wang *et al.* used DBD plasma in an O<sub>2</sub>/N<sub>2</sub> mixture to prepare a Pt/CeO<sub>2</sub> catalyst [147]. The plasma-treated catalyst reduced T<sub>90</sub> (the temperature to get 90% conversion) from 287 °C to 208 °C for toluene oxidation. TEM and CO pulse chemisorption revealed smaller particle size, higher dispersion, Ce<sup>3+</sup> amounts, and higher oxygen vacancies as a result of DBD plasma treatment. Pastor-Perez *et al.* found that Ar plasma-treated Pt/CeO<sub>2</sub> catalysts exhibited higher performance in the water-gas shift reaction (WGS) [141]. XPS and XANES analyses revealed that plasma treatment generated electron-enriched Pt NPs which showed a very strong interaction with the CeO<sub>2</sub> support. The enhanced metal-support interaction of Pt/TiO<sub>2</sub> was also reported by Zou *et al.* [148], who treated a catalyst with a low-pressure DC Ar glow discharge at 100 Pa. Xu *et al.* applied O<sub>2</sub> plasma to an Au/CoO<sub>x</sub>/SiO<sub>2</sub> catalyst and found good CO oxidation activity due to the size reduction and good dispersion of plasma-treated metal NPs [149]. Wang *et al.* reported that O<sub>2</sub> plasma-treated carbon black (CB) exhibits electrochemical generation of hydrogen peroxide with 100% Faradaic efficiency [150]. The current density reached  $0.44 \text{ mA cm}^{-2}$  at the theoretical potential of H<sub>2</sub>O<sub>2</sub> generation, and the mass activity ( $300 \text{ A g}^{-1}$ ) was the highest among state-of-the-art catalysts. Microscopic and spectroscopic characterization as well as DFT calculations, indicated that the performance was due to the defective carbon structure after plasma treatment.

Rapid advances in state-of-the-art analytical technology have enabled the visualization of atomic-scale dynamics of metal NPs under realistic reaction conditions. This information also suggests that a variety of changes in metal NPs that have been experimentally observed may possess high potential for tailored preparation of catalysts with higher activity and better stability. The examples presented in this section demonstrate only the tip of the iceberg. We believe that the smart coupling of plasma-catalyst interaction is not limited to direct activation of catalysts, but catalyst preparation and regeneration of deactivation should also be further explored in the future.

**Table 2.** Effect of plasma on the catalyst during the catalyst preparation.

| CAT  | Plasma conditions |                                |                       | Remarks  | Ref   |
|--|-------------------|--------------------------------|-----------------------|--|-------|
|  | pressure          | gas                            | plasma                |  |       |
| Au/SiO <sub>2</sub>                        | 400 mTorr         | O <sub>2</sub>                 | RF                    | Small size (~ 3 nm),<br>selective hydrogenation of C <sub>2</sub> H <sub>2</sub> ,<br>optimized neutral surface charge of the Au NPs | [138] |
| Au/CoO <sub>x</sub> /SiO <sub>2</sub>      | 1 atm             | O <sub>2</sub>                 | RF                    | Smaller size, higher dispersion  | [149] |
| Au/TiO <sub>2</sub>                        | 1 atm             | O <sub>2</sub>                 | DBD                   | Small size with narrow size distribution,<br>large amount of low-coordinated Au species  | [151] |
| Pt/CeO <sub>2</sub>                        | 0.15 Torr         | Ar                             | RF glow               | Electron-enriched Pt particles with very<br>strong interaction with the ceria support,   | [141] |
| Pt/CeO <sub>2</sub>                        | 1 atm             | O <sub>2</sub> /N <sub>2</sub> | DBD                   | Smaller Pt size with higher dispersion,<br>high concentration of O <sub>2</sub> vacancies and Ce <sup>3+</sup>                       | [147] |
| Pt/TiO <sub>2</sub>                        | 1 atm             | H <sub>2</sub> /Ar             | DBD                   | Complete reduction of Pt NPs,<br>smaller size with higher dispersion,<br>enhanced M-support interaction                              | [152] |
| Pt/TiO <sub>2</sub>                        | 100 Pa            | Ar                             | DC glow               | Good photocatalyst for H <sub>2</sub> production,<br>Enhanced metal-support interaction  | [148] |
| Pt/NaZSM-5                                 | 50-150 Pa         | Ar                             | DC glow <sup>1)</sup> | Good dispersion,<br>good NO reduction with CH <sub>4</sub>   | [144] |
| Pd/FeO <sub>x</sub>                        | 1 atm             | H <sub>2</sub>                 | DBD                   | Higher metallic Pd ratio,<br>abundant oxygen vacancies,<br>enhanced low temperature CO oxidation                                     | [140] |
| PdO/Alumina                                | 100-200 Pa        | Ar                             | DC Glow <sup>2)</sup> | Lower light-off temperature for CH <sub>4</sub> combustion   | [153] |
| HfN <sub>x</sub> O <sub>y</sub>            | 1 atm             | Air, N <sub>2</sub>            | DBD                   | Comparable to Pt as electrocatalyst  | [154] |
| Co-Pt<br>/γ-Al <sub>2</sub> O <sub>3</sub> | 50 Pa             | N <sub>2</sub> →H <sub>2</sub> | Glow                  | Good metal dispersion  | [155] |
| M on three<br>supports <sup>3)</sup>       | 100 Pa            | Or, Ar                         | DC glow               | Reduction of metal ions to metals,   | [156] |
| Ni on three<br>supports <sup>4)</sup>      | 1 atm             | Air                            | DBD                   | Plasma produces mainly Ni(111) with fewer<br>defect,<br>Improved coke resistance   | [157] |
| Ni/γ-Al <sub>2</sub> O <sub>3</sub>        | 1 atm             | Ar                             | AC                    | Increase in CH <sub>4</sub> conversion (5-10%),<br>preventing carbon deposition on Ni  | [158] |

<sup>1,2)</sup> Glow plasma followed by thermal calcination: <sup>3)</sup> M = Pt, Pd, Ag, Au, supports = TiO<sub>2</sub>, γ-Al<sub>2</sub>O<sub>3</sub>, HZSM-5:

<sup>4)</sup> supports = MgO, SiO<sub>2</sub>, MgAl<sub>2</sub>O<sub>4</sub>,

## 4.2 Challenge: *operando in situ* diagnostics

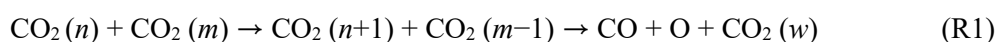
Advances in analytical instruments allow the measurement of unstable intermediates, structural changes, and redox conditions, which is helpful for gaining a deeper understanding of the reaction mechanism. As discussed in the previous section, several examples of *in situ* and/or *operando* diagnostic tools have been developed to capture the atomic-scale dynamics of the catalyst surface. *Operando* measurement is a technical term for measuring surface phenomena on catalysts under realistic reaction conditions [159–161]. To date, a number of methods have been developed for *operando* spectroscopy, including Raman, UV, FTIR, X-ray adsorption, XRD, ETEM, ambient pressure XPS (AP-XPS), and ambient pressure scanning tunnel microscopy (AP-STM). Synchrotron radiation spectroscopy has become a cutting-edge technique for *operando* measurement of catalysis. Vamvakeros *et al.* measured five-dimensional (three spatial, one scattering, and one time/imposed state) tomographic diffraction imaging of a multi-component catalyst (Ni–Pd/CeO<sub>2</sub>–ZrO<sub>2</sub>/Al<sub>2</sub>O<sub>3</sub>) under different gas mixtures (He, H<sub>2</sub>/He, O<sub>2</sub>/He, CH<sub>4</sub>/O<sub>2</sub>) [162]. The non-destructive *operando* XRD-CT (computed tomography) technique enables *in situ* imaging of the phase and structural changes of metals and supports by unveiling the elementary steps of the catalytic reaction.

In conjunction with the five matching issues and tailored design of plasma catalysis, a good understanding of the surface structure and its transit morphology is essential to elucidate numerous uncertainties remaining in the interaction of plasma with the catalyst. However, the number of surface measurement techniques available for plasma catalysis is limited. Extension of these techniques to plasma catalysis usually requires significant modification, mostly due to the presence of high-voltage and electromagnetic noise from plasmas. Non-intrusive measurements are the first option for plasma catalysis. Synchrotron X-rays have also been employed in plasma catalysis to measure the dynamic changes of catalysts under plasma activation. For example, Gibson *et al.* [163] employed X-ray absorption fine structure (XAFS) for CH<sub>4</sub> oxidation over a Pd/Al<sub>2</sub>O<sub>3</sub> catalyst and observed no meaningful changes in the extended X-ray absorption fine structure (EXAFS). However, they estimated the heating of Pd NPs from the amplitude of the EXAFS oscillations and concluded that the Pd temperature rise was insufficient to activate the thermal CH<sub>4</sub> oxidation reaction.

One of the rapid modifications made for plasma catalysis is operando FTIR or diffuse reflectance infrared FTIR spectrometry (DRIFTS). Turan *et al.* [164] reported DBD coupled DRIFTS for measuring water desorption from KBr within a 1 min interval. Rivallan *et al.* applied the operando IR technique to measure the oxidation of isopropanol (IPA) on  $\gamma$ -Al<sub>2</sub>O<sub>3</sub> by DBD [165]. Knoll *et al.* [166] measured CH<sub>4</sub> oxidation over an alumina/silica-supported Ni catalyst using a DRIFT system coupled with an Ar/O<sub>2</sub> plasma jet. They postulated that the surface carboxylate group (COO<sup>-</sup>) is closely involved in the conversion of CH<sub>4</sub> to CO and CO<sub>2</sub>. Stere *et al.* [167] used DRIFTS coupled with mass spectroscopy (DRIFTS-MS) to determine the surface species during the hydrocarbon-SCR reaction over Ag/Al<sub>2</sub>O<sub>3</sub>. Sheng *et al.* [168] measured CH<sub>4</sub> reforming with CO<sub>2</sub> over a Ni-La/Al<sub>2</sub>O<sub>3</sub> catalyst and showed that plasma activation resulted in 1.7 times increase in the formation of bidentate (1560 and 1290 cm<sup>-1</sup>) and monodentate carbonate (1425 and 1345 cm<sup>-1</sup>). Moreover, new peaks of bicarbonate (1655 cm<sup>-1</sup>) and bridge carbonate (1720 cm<sup>-1</sup>) were formed because of NPT interactions. Rodrigues *et al.* also applied operando DRIFTS to trace the intermediates during the oxidation of IPA and toluene over metal oxides ( $\gamma$ -Al<sub>2</sub>O<sub>3</sub>, TiO<sub>2</sub> and CeO<sub>2</sub>) [169]. Oxidation of PM over Au/ $\gamma$ -Al<sub>2</sub>O<sub>3</sub> was monitored by Lu *et al.* using *in situ* plasma DRIFTS-MS [170]. We find that DRIFT measurement will be one of must-have analytic tools for various plasma catalysis reactions in the near future.

### 4.3 Finding effective catalyst for the vibrationally excited molecules

Plasma is generated and sustained through electron-molecules collisions. NTP is characterized by electrons with kinetic energies much higher than those of ions and gas molecules. The high-energy electrons undergo multiple inelastic collisions with the dominant gas molecules to produce ionization and excitation. Fig. 17 shows the typical fractions of electron energy in NTP reactor. The mean energy of the electrons found in most NTP reactors is below 10 eV. In this energy range, most of the electron energy is dissipated to form vibrationally excited molecules. It should be noted that the direct electron impact pathway for the dissociation/decomposition of pollutants in the ppm range could not constitute a major mechanism. Energy costs to generate particles are simple to estimate for vibrational  $\ll$  electronic  $\ll$  ionization, so the effective utilization of vibrational energy is the key to making plasma catalysis energy-effective. The importance of using vibrational energy to improve energy efficiency was already pointed out in the early 1990s [171]. However, there have been relatively few reports of direct experimental evidence supporting the significant role of hot (vibrationally, translationally excited) molecules in gas-phase reactions. Two-photon absorption laser-induced fluorescence (TALIF) measurements of two consecutive pulses clearly demonstrated that vibrationally excited N<sub>2</sub> molecules, N<sub>2</sub>( $\nu$ ), enhanced the formation of N atoms when the interval between the first and second pulses was less than 300  $\mu$ s [172]. Homogeneous CO<sub>2</sub> dissociation by vibration-to-vibration energy transfer is explained by the ladder-climbing mechanism [173–175]. The most important vibration mode is the asymmetric stretching vibration:



Here,  $n$ ,  $m$ , and  $w$  denote asymmetric vibrational quantum numbers. Vibrationally excited CO<sub>2</sub> is produced by the electron impact in NTP. Multiple collisions between vibrational CO<sub>2</sub> lead to dissociation into CO and O when the vibrational quantum number exceeds  $\nu = 21$  which corresponds to the CO<sub>2</sub> dissociation limit (5.52 eV) [176]. To ensure such high collision frequency, high-pressure NTP such as DBD and gliding arc discharge are desired. The vibrational ladder-climbing mechanism is more efficient than the direct dissociation pathway

because energy transfer between  $\text{CO}_2(n)$  and  $\text{CO}_2(m)$  occurs efficiently without excess energy transfer into the electronically excited state of  $\text{CO}_2$ . However, there is a trade-off between energy efficiency and  $\text{CO}_2$  conversion: the production of a higher vibrational state ( $\text{CO}_2(n+1)$ ) inevitably accompanies the deactivation of the counter molecule ( $\text{CO}_2(m-1)$ ). This trade-off relationship is observed in DBD, gliding arc discharge, and microwave plasma, as presented in recent review papers [177, 178].

Yamazaki *et al.* have performed a kinetic study of plasma-activated  $\text{CO}_2$  dissociation using low-pressure recombining hydrogen plasma [179]. They selected this unique plasma as an extremely low-energy electron plasma source that is suitable for  $\text{CO}_2$  vibrational activation and minimizes the inefficient direct dissociation process. Moreover, they performed comprehensive *in situ* plasma diagnostics of the recombining plasma, showing an electron density;  $10^{18}$ – $10^{19} \text{ m}^{-3}$  and a mean electron energy of 0.15–0.45 eV at 8.8 Pa. Vibrational ladder-climbing via multiple electron collisions becomes the dominant pathway because of the low gas pressure and high electron density:



Unlike high-pressure NTP such as DBD and gliding arc discharge, vibration-vibration (V–V) energy transfer is inefficient in low-pressure recombining plasma. Meanwhile, the electron-induced ladder-climbing mechanism is possible, yielding a  $\text{CO}_2$  conversion as high as 60%. Their study implicates the necessity of a new plasma source for efficient  $\text{CO}_2$  splitting via an electronic process: a low-energy and high-density electron plasma would break the limitation of the trade-off between  $\text{CO}_2$  conversion and energy efficiency via an electron-induced ladder-climbing pathway. Vibrationally excited molecules are populated in the gas phase via a ladder-climbing mechanism, which further contributes to and promotes surface reactions when heterogeneous catalysts are combined.

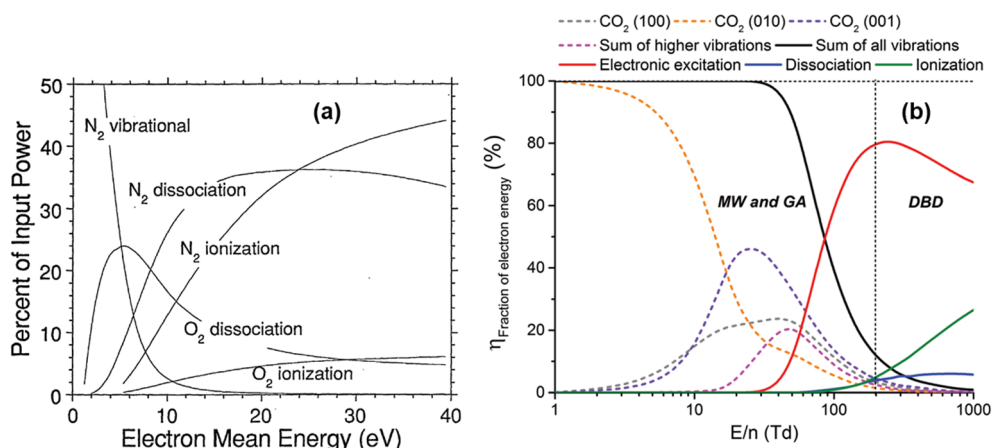


**Fig. 17.** Energy dissipation in electron-molecule collision: (a) dry air [180] courtesy of Copyright (1997) The Physical Society of Japan and The Japan Society of Applied Physics, (b)  $\text{CO}_2$  [177] with permission from The Royal Society of Chemistry (RSC).

The dissociation of chemical bonds depends on the bond strength, which is closely related to the internal energy state. Fig. 18 illustrates two representative cases in which vibrational energy plays a role in the surface chemistry. One is the so-called (a) collision of hot molecules that are in either a vibrationally or rotationally excited state. This topic has long been the subject of molecular beams, which are discussed below. The second type is (b) vibrational excitation of adsorbed molecules by the energy exchange of plasma-induced particles (photons, electrons, and excited molecules). Oh *et al.* observed the lateral hopping of a CO molecule on Ag(110) using action spectroscopy with a scanning tunneling microscope (STM-AS) [181]. Once molecules are vibrationally activated, regardless of the position at which they are activated, a substantial increase in reaction rate can be obtained. Marinov *et al.* [46] experimentally measured the deactivation probability of vibrationally excited  $\text{N}_2$  on various surfaces using infrared titration combined with quantum cascade laser absorption spectroscopy. The probability of deactivation depended on the type of materials: silica ( $5.7$ – $11 \times 10^{-4}$ ) > Pyrex ( $6$ – $11 \times 10^{-4}$ ) >  $\text{Al}_2\text{O}_3$  ( $5.7$ – $11 \times 10^{-4}$ ) > anodized Al ( $291 \times 10^{-4}$ ) >  $\text{TiO}_2$  film ( $19 \times 10^{-4}$ ). However, these values can be greatly enhanced when the surface is replaced by active metal NPs.

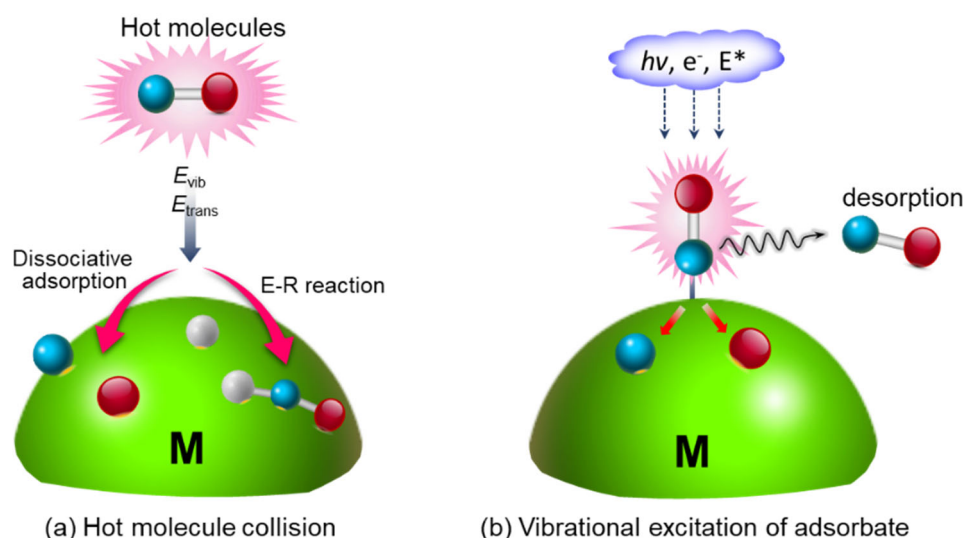


**Fig. 18.** Promoting chemical reactions through kinetic energy: (a) hot molecule collision, (b) vibrational excitation of adsorbed molecules by energy exchange from incident photons, electrons, and excited molecules.

Molecular beam techniques, especially energy-state resolved molecules, have provided useful basic information regarding dissociative adsorption, energy barriers of impinging molecules for a given surface, and desorption. Fig. 19 shows an example of excited hot molecules enhancing the absolute sticking probability of  $\text{CH}_4$  on a clean Ni(100) surface [182]. When the  $\text{CH}_4$  molecules were excited (open circles in the figure) with an infrared laser to the  $\nu_3$  mode, a dramatic enhancement in the initial sticking probability was observed for all tested energy ranges. It was also observed that the initial reaction probability increased with the incident kinetic energy of  $\text{CH}_4$  impinging on the clean Ni(111) surface [183]. The isotope-labeled experiment ( $\text{CHD}_3$ ) revealed that the initial reaction probability of dissociative chemisorption on Ni(111) increased by a factor of  $\sim 10^3$  when the translational energy was increased from approximately  $50 \text{ kJ mol}^{-1}$  to  $90 \text{ kJ mol}^{-1}$ . The same group later compared the initial reaction between vibrational energy ( $E_{\text{vib}}$ ) and translational energy ( $E_{\text{trans}}$ ) and provided a clear conclusion that  $E_{\text{vib}}$  is more effective than  $E_{\text{trans}}$  in promoting the reactivity of  $\text{CH}_4$  on clean Ni(111) [184]. Juurlink *et al.* indicated that  $\text{CH}_4$  molecules excited to  $\nu = 1$  of the  $\nu_3$ -CH stretching vibration are up to 1600 times more reactive on a clean Ni(100) surface than molecules in the ground state [182]. Bisson *et al.* compared the reactivity of  $\text{CH}_4$  ( $2\nu_3$ ) on Pt(111) and Ni(111) and found that Pt(111) has a much higher sticking coefficient [185]. It must be mentioned that the saturated coverage by  $\text{CH}_3$  and H on these metal surfaces is not influenced by vibrational excitation [186]. When the catalyst surface is saturated by rapid chemisorption via plasma, further  $\text{CH}_4$  conversion is not possible. In fact, plasma-induced synergy for  $\text{CH}_4/\text{CO}_2$  reforming over Ni/ $\text{Al}_2\text{O}_3$  has not been clearly observed [187]. In contrast, a synergistic effect was obtained using a La-Ni/ $\text{Al}_2\text{O}_3$  catalyst because  $\text{CO}_2$  is activated by plasma simultaneously, which increases mono- and bidentate carbonates over La to react with neighboring adsorbed  $\text{CH}_4$  fragments. Active sites for  $\text{CH}_4$  are regenerated and thus overall  $\text{CH}_4$  and  $\text{CO}_2$  conversion are increased by plasma; cooperative activation of  $\text{CH}_4$  and  $\text{CO}_2$  together with appropriate combination of catalysts is critically important.

Recently, Quan *et al.* indicated that vibrational energy was more effective than translational energy in the Eley-Rideal type dissociative adsorption of  $\text{CO}_2$  on a model surface of Cu(111) and Cu(100) [188]. They also indicated a mode-selective result in which bending mode dominated over the symmetric and asymmetric stretching modes. Furthermore, the reaction rate was independent of the surface temperature and was found to be a function of the vibrational energy of  $\text{CO}_2$ . This is a very striking conclusion because the energy state of the impinging molecules determines reactivity rather than the surface temperature. The effective surface accommodation of vibrationally excited molecules may depend on the nature of the surface. Despite some clear evidence in molecular beam studies, the efficient utilization of these vibrationally excited molecules remains an unexplored area. If we can realize the effective utilization of vibrationally excited molecules, a ground-breaking process can be established. The development of a nanosecond pulse power supply (output voltage up to 30 kV, pulse width  $< 20 \text{ ns}$ , and frequency  $10^4 \sim 10^5 \text{ Hz}$ ) is necessary to distinguish the contribution of heating and hot molecules in plasma catalysis.

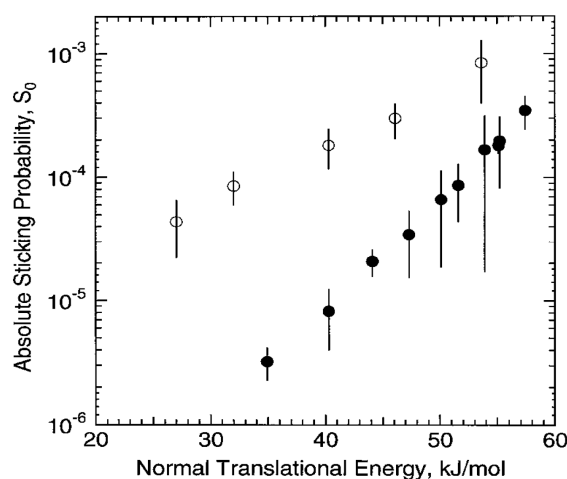


**Fig. 19.** Vibrationally averaged sticking probabilities for CH<sub>4</sub> on a clean Ni(100) surface with (open circles) and without (solid circles) laser excitation of the  $J = 2$ ,  $\nu_3$  C-H stretching eigenstate. With the permission of APS.

#### 4.4 Newly emerging materials (examples in NH<sub>3</sub> synthesis)

Developing plasma catalysis free from PGMs could be an attractive route to pursue. As indicated in Section 2.1.5, plasma catalysis has the potential to utilize materials that are considered less active. For example, Yan *et al.* recently reported hafnium (Hf) as a possible alternative to Pt for water electrolysis. They first treated Hf using DBD in air and then switched to N<sub>2</sub> plasma to obtain hafnium oxyhydroxide (HfN<sub>x</sub>O<sub>y</sub>), which is comparable to Pt as an electrocatalyst for hydrogen production from water electrolysis [154]. A very similar strategy has been applied for O incorporation in MOS<sub>2</sub>, which can also substitute Pt as an electrocatalyst for H<sub>2</sub> formation [139]. Pt has also been widely used for the oxidation of hydrocarbons because of the superior catalytic activity and excellent durability. However, in the plasma catalytic oxidation of VOCs, Ag can achieve similar or even better activity [189]. Considering the rapid transition from fossil fuels to clean energy in the near future, the substitution of PGMs will be more heavily focused on energy-related topics.

The Haber-Bosch process has been used for ammonia synthesis for more than 100 years, but it still attracts attention from researchers and society. Recently, various new materials have been developed and tested as new possible supports for Ru catalysts. Fig. 20 compares the space time yield (STY) in ammonia synthesis. The (mmol g<sup>-1</sup> h<sup>-1</sup>), the amount of product per unit time per unit weight of catalyst, is an important measure of catalytic activity for a given reaction. The STY is also a type of reaction rate normalized with the amount of catalyst used.

$$\text{STY} = \frac{[C_i]_{in} - [C_i]_{out}}{g_{CAT} h} \quad (9)$$

[C<sub>i</sub>],  $g_{CAT}$ , and  $h$  represent the molar concentration of species  $i$ , amount of catalyst (g), and space velocity, respectively. Ru appears to be the most popular active metal. One noticeable recent trend is the development of new materials for supports that have never previously been investigated. These include electride [190, 191], Pr<sub>2</sub>O<sub>3</sub> [192], BaO·6Al<sub>2</sub>O<sub>3</sub> (BHA: barium hexaaluminate) [193], Ba-Ca(NH<sub>2</sub>)<sub>2</sub> [194], and La<sub>0.5</sub>Ce<sub>0.5</sub>O<sub>1.75</sub> [195]. By 2000, an STY of 1000 μmol g<sup>-1</sup> h<sup>-1</sup> was a measure of the high performance of NH<sub>3</sub> synthesis at 0.1 MPa. Substantial enhancement from the μmol to mmol level has been achieved over the last 10 years. As plasma parameters are not considered in STY, energy-related evaluation is also required for plasma catalysis. One of the widely used metrics in plasma chemistry is energy yield, which measures energy consumption (kWh) to obtain the unit weight of ammonia (g-NH<sub>3</sub>). However, one should be aware of the meaning and limitation of energy yield because it is only valid for the range in which a linear correlation between conversion and SIE is guaranteed (Ref. [196] and supporting information). Barboun *et al.* [197] achieved 3.6 mmol g<sup>-1</sup> h<sup>-1</sup> with M (M = Ni, Co)/γ-Al<sub>2</sub>O<sub>3</sub> at 20 kJ L<sup>-1</sup>. Li *et al.* [198] observed a linear relationship between NH<sub>3</sub> concentration (~10800 ppm) and SIE (~15 kJ L<sup>-1</sup>) with Ru(5)/α-Al<sub>2</sub>O<sub>3</sub> and the resulting STY was approximately 16.4 mmol g<sup>-1</sup> h<sup>-1</sup>. However, the energy yield was about 3.1 g-NH<sub>3</sub> kW<sup>-1</sup>h<sup>-1</sup>. According to the analysis performed by Rouwenhorst *et al.* [199], the energy yield versus NH<sub>3</sub> concentration shows a bell-shaped curve and the

maximum value is about  $36 \text{ g-NH}_3 \text{ kW}^{-1} \text{ h}^{-1}$  at 0.2%  $\text{NH}_3$  concentration [196]. The  $\text{NH}_3$  synthesis reaction favors high pressure, which is still an unexploited area for plasma catalysis. According to the electrocatalytic  $\text{NH}_3$  synthesis performed by Manabe *et al.* [200], an STY of  $30 \text{ mmol g}^{-1} \text{ h}^{-1}$  with an energy yield of  $36.3 \text{ g-NH}_3 \text{ kW}^{-1} \text{ h}^{-1}$  was obtained at 0.9 MPa. It is interesting to see how the pressure-dependent behavior of plasma catalysis affects energy yield, the bell-shaped curve, and the maximum  $\text{NH}_3$  concentration.

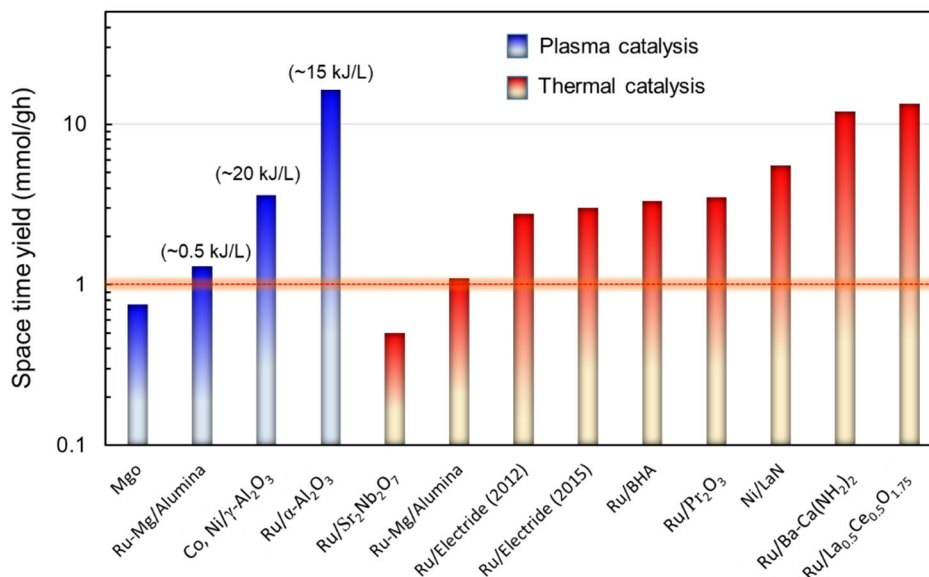


**Fig. 20.** Comparison of STY in ammonia synthesis at 0.1 MPa. Thermal catalysis adopts  $\text{H}_2/\text{N}_2 = 3$ , whereas for plasma catalysis  $\text{H}_2/\text{N}_2 = 0.2\text{--}0.3$ .

A typical drawback of Ru catalysts is poisoning by hydrogen, which mitigates the benefits of high pressure. However, Ru on electride and  $\text{La}_{0.5}\text{Ce}_{0.5}\text{O}_{1.75}$  can avoid hydrogen poisoning and lead to higher  $\text{NH}_3$  yields at higher pressures. Ogura *et al.* reported an STY of  $13.4 \text{ mmol g}^{-1} \text{ h}^{-1}$  with  $\text{Ru}/\text{La}_{0.5}\text{Ce}_{0.5}\text{O}_{1.75}$ , which is the highest value obtained with a Ru catalyst. They further indicated that the STY increased with pressure to  $31.3 \text{ mmol g}^{-1} \text{ h}^{-1}$  (1.0 MPa) and  $44.4 \text{ mmol g}^{-1} \text{ h}^{-1}$  (3.0 MPa) without saturation or decrease. Catalyst characterization using HAADF-STEM and EDX mapping, electron energy loss spectroscopy (EELS), and IR spectroscopy revealed that the Ru NPs were partially covered with the thermostable support ( $\text{La}_{0.5}\text{Ce}_{0.5}\text{O}_{1.75}$ ) and the cooperative interaction for  $\text{N}_2$  dissociation at the interface was suggested as a plausible mechanism for the high yield of  $\text{NH}_3$ . In 2020, Hosono's group at the Tokyo Institute of Technology reported a remarkable  $\text{NH}_3$  yield with Ni-loaded lanthanum nitride (Ni/LaN) [201]. In conventional works, Ni has been considered a less active metal for  $\text{NH}_3$  synthesis, but a significant enhancement was achieved by combining it with LaN owing to a dual-site mechanism. Nitrogen vacancies in LaN were found to be active for the dissociation of  $\text{N}_2$ , which is the rate-determining step for all  $\text{NH}_3$  synthesis reactions. Ni metal NPs loaded onto the nitride dissociated  $\text{H}_2$ . The dual sites for activating  $\text{N}_2$  and  $\text{H}_2$  separately were the key factors enabling the Ni catalyst to be comparable with the Ru-based catalysts.

Binary and ternary catalysts can broaden the scope of plasma catalysis as has already been proven in the conventional thermal catalysis. As mentioned in Section 2.1.5, the combination of two ubiquitous metals that can substitute PGMs will be an important avenue for plasma catalysis. Data accumulation of dynamics on the metal NPs under plasma application may accelerate the development of new catalysts tailored for plasma catalysis. Although the number of examples is still limited insofar, "activity inversion" suggests that material screening needs to be performed in a wider spectrum than expected from the literature for thermal catalysis.

#### 4.5 Arrhenius plot and activation energy

The Arrhenius plot is widely used to determine the activation energy for a given catalytic reaction. As the temperature increases, the proportion of molecules that can overcome the energy barrier increases. The energy barrier (i.e., activation energy  $E_a$  in  $\text{kJ mol}^{-1}$ ) indicates the minimum energy required to initiate a given reaction, as indicated in Fig. 21 (a). Catalysts can increase the reaction rate by providing a new pathway that has smaller

$E_a$  compared to the uncatalyzed reaction. A large activation energy indicates that a high gas temperature is required to overcome the reaction barrier. In the case of reactions dominated by rapid radical chemistry, the activation energy can take a zero value, indicating no temperature-dependent behavior. However, most catalytic reactions mediated by surface active sites have activation energies determined by the slowest process in all elementary steps. The decrease in  $E_a$  in plasma catalysis can be interpreted as the plasma-driven pathway dominating over the thermal-driven pathway. As mentioned in the previous section, vibrational excitation can also promote the reaction, as is expressed in Eq. (10).

$$k_{vib} = A \exp\left(-\frac{E_a - \eta E_a^v}{RT}\right) \quad (10)$$

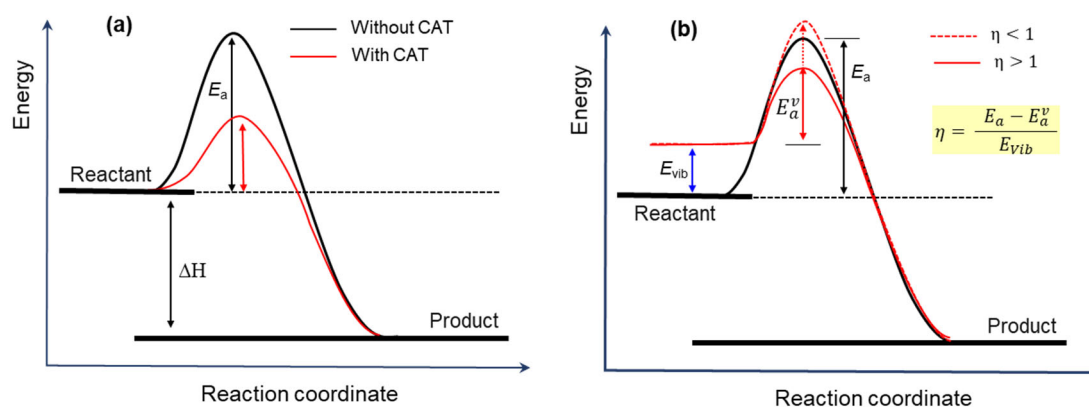


**Fig. 21.** Activation energies in (a) thermal reaction, and (b) contribution of vibrational energy in plasma catalysis.

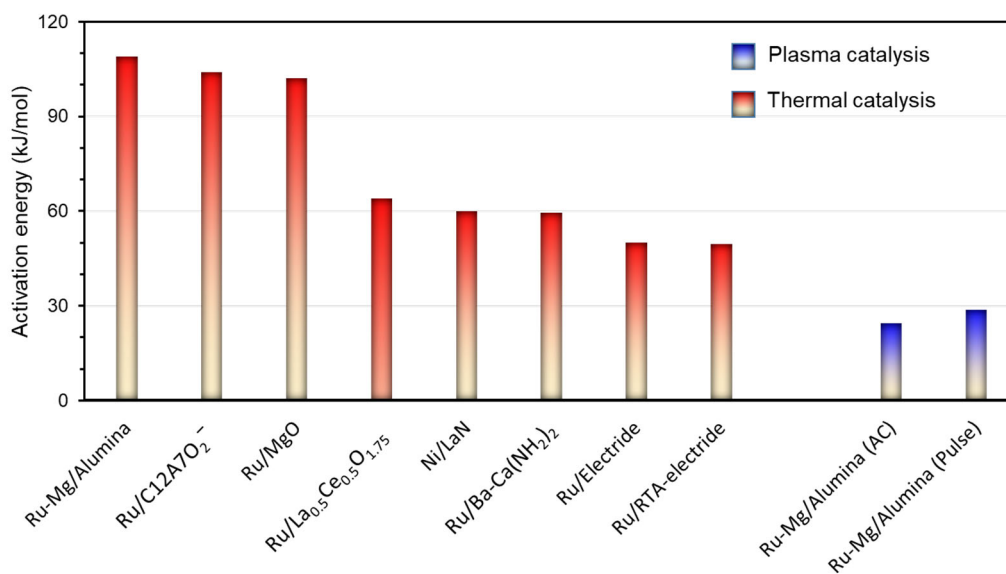
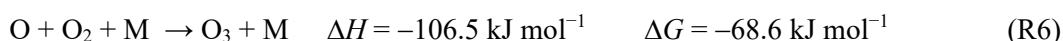
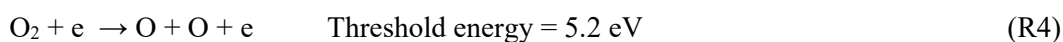


**Fig. 22.** Comparison of activation energies in ammonia synthesis at 0.1 MPa.

Fig. 22 presents the activation energies for  $\text{NH}_3$  synthesis for both thermal and plasma catalysis. Conventional  $\text{C12A7:O}^{2-}$  has an activation energy of  $104 \text{ kJ mol}^{-1}$ . Kanbara *et al.* indicated that the performance of Ru-loaded electride ( $\text{C12A7:e}^-$ ) depends significantly on the degree of electron substitution for  $\text{O}^{2-}$  anions, and observed a decrease in the activation energy from  $110 \text{ kJ mol}^{-1}$  to  $50 \text{ kJ mol}^{-1}$  under optimum conditions [191, 202]. For the Ni/LaN NP catalyst, the rate-determining step was the combination of  $\text{H}^*$  and  $\text{N}_{\text{lattice}}$ . The experimentally measured activation barrier ( $60 \text{ kJ mol}^{-1}$ ) was consistent with the computed energy barrier of hydrogenation of  $\text{N}_{\text{lattice}}$  ( $0.54 \text{ eV}$  or  $52.1 \text{ kJ mol}^{-1}$ ). In the case of plasma catalysis, the activation energy was found to be  $24.4 \text{ kJ mol}^{-1}$  and  $28.7 \text{ kJ mol}^{-1}$  for AC pulse energization, respectively. Murakami *et al.* [203] studied electrocatalytic synthesis of  $\text{NH}_3$  with a Cs(9.9)-Ru(5.0)/SrZrO<sub>3</sub> catalyst, albeit slightly different from plasma catalysis, and reported activation energies of  $107.0 \text{ kJ mol}^{-1}$  and  $38.2 \text{ kJ mol}^{-1}$

without and with an e-field, respectively. A similar drop in activation energy was reported in plasma catalysis for CO<sub>2</sub> methanation, where the  $E_a$  values for thermal reaction and plasma catalysis were 82 kJ mol<sup>-1</sup> and 21 kJ mol<sup>-1</sup>, respectively [204]. On the other hand, non-Arrhenius behavior was reported for dry reforming of CH<sub>4</sub> with CO<sub>2</sub> over Ni/γ-Al<sub>2</sub>O<sub>3</sub> by Kim *et al.* [205], where the activation energy remained constant over the tested temperature range and plasma input power (1-7 W).

Although the Arrhenius plot and activation energy can provide some insight into plasma catalysis, one important unsolved question is about “temperature”. A rift still exists between catalysis and plasma in using the term “temperature”. It should be noted that the Arrhenius plot in thermal catalysis is considered to be under thermal equilibrium conditions. However, different levels of temperature coexist in NTPs: extremely high electron temperature ( $T_e > 10^4$  K), vibrational temperature ( $T_{\text{vib}} = 10^2 \sim 10^3$  K), rotational temperature ( $T_{\text{rot}} \sim 10^2$  K), and translational and gas temperature ( $T_g = T_{\text{trans}} < 10^2$  K). This non-equilibrium nature of plasma means plasma catalysis can even exceed the thermal equilibrium limit [206, 207]. This is not surprising if we remember that plasma is the only technique for O<sub>3</sub> production on an industrial scale. Ozone (O<sub>3</sub>) generation, which is not produced thermodynamically under ambient conditions (R3:  $\Delta G > 0$ ), has long been a good example of how the non-equilibrium nature of plasma can overcome thermodynamic limitations. It must be also mentioned that NTP does not break the law of physics: ozone synthesis via R6 occurs spontaneously ( $\Delta G < 0$ ); obviously, the role of NTP is to dissociate O<sub>2</sub> into O + O (R4) by a method other than using thermal energy (R5:  $\Delta G = 231.8$  kJ mol<sup>-1</sup>). The key issue is to promote R4 kinetically and not thermodynamically. Because R4 can be formulated as a temperature ( $T_g$ ) independent term, the apparent activation energy in the conventional Arrhenius expression can yield an unexpectedly small value of  $E_a \approx 0$  kJ mol<sup>-1</sup>. As discussed in Section 4.5, analysis of the Arrhenius curve and the interpretation of the activation energy must be carefully performed. In the case of the two-temperature model where vibrational and translational temperatures are different, the individual contributions of  $T_g$  and  $T_{\text{vib}}$  can be formulated using modified Arrhenius expression by finding  $T_g$  and  $T_{\text{vib}}$  experimentally. This theoretical treatment of plasma catalysis emphasizes the necessity of new plasma diagnostic methods to determine the vibrational temperature of target molecules. The theoretical treatment of V-V and V-T transition kinetics must be further improved.



The electron temperature is the primary tuning knob to control the radical production rate in the gas phase; however,  $T_e$  is not directly coupled with surface reaction chemistry and, thus, the contribution of  $T_e$  is not formulated in the Arrhenius expression. Meanwhile, the number density of vibrationally excited molecules in different vibrational quanta is correlated to  $T_{\text{vib}}$  assuming Boltzmann distribution, yet  $T_{\text{vib}}$  and  $T_g$  take different values in NTP. This unique contribution of  $T_{\text{vib}}$  has been studied in molecular beam research, providing useful and insightful reaction kinetics involving vibrationally excited molecules. One debate has yet to be solved: the molecular beam study does not provide a technical approach to generate abundant vibrationally excited molecules without increasing the temperature of the entire reaction system. Laser-induced vibrational excitation is not practical because of the cost. Moreover, the laser does not penetrate and is not accessible to packed-bed catalysts in a reactor. Obviously, NTP provides a scalable and viable solution.

Sheng *et al.* have performed a kinetic analysis of CH<sub>4</sub> dry reforming ( $\text{CH}_4 + \text{CO}_2 = 2\text{CO} + 2\text{H}_2$ ) in a PB-DBD reactor. Reaction orders, activation energy, and the contribution of vibrationally excited CH<sub>4</sub> were experimentally validated and correlated with mode-selective vibrational activation of CH<sub>4</sub> and its reactivity over metal surfaces [208]. First, the plasma did not change the reaction orders for CH<sub>4</sub> and CO<sub>2</sub> because the saturated surface coverage was not influenced by vibrational excitation [186]. The activation energy for 12 kHz DBD (83.2 kJ mol<sup>-1</sup>) was slightly decreased compared to in thermal catalysis (91.2 kJ mol<sup>-1</sup>), whereas the reaction rate constant obviously increased. Reaction promotion was possible temporarily during streamer propagation, but the catalyst surface was not fully covered by the streamer swarm [62]. Moreover, during the DBD-off period over the cycle, plasma-induced synergy was obviously absent. This fact implies that we

observed a mixture of thermal and plasma catalysis, which is defined as mixed catalysis in Ref. [208]: overall  $\text{CH}_4$  conversion is increased by the superposition of DBD, but the reaction is essentially dominated by thermal catalysis. A similar reaction behavior was observed for  $\text{CH}_4$  steam reforming [209]. When 100 kHz DBD was applied, the activation energy decreased dramatically from  $91.2 \text{ kJ mol}^{-1}$  to  $44.7 \text{ kJ mol}^{-1}$ . The lifetime (V-T transition decay time) of bending-mode  $\text{CH}_4$  at 873 K and 5 kPa was estimated to be  $31 \mu\text{s}$ , while gas breakdown occurred every  $5 \mu\text{s}$  at 100 kHz: bending-mode  $\text{CH}_4$  was accumulated in the reactor and continuously reacted on the catalyst including during the DBD-off period. In the case of 12 kHz DBD, the DBD-off duration ( $42 \mu\text{s}$ ) is longer than the lifetime of the bending-mode  $\text{CH}_4$ ; vibrationally excited species are fully deactivated or consumed during the DBD-off period.

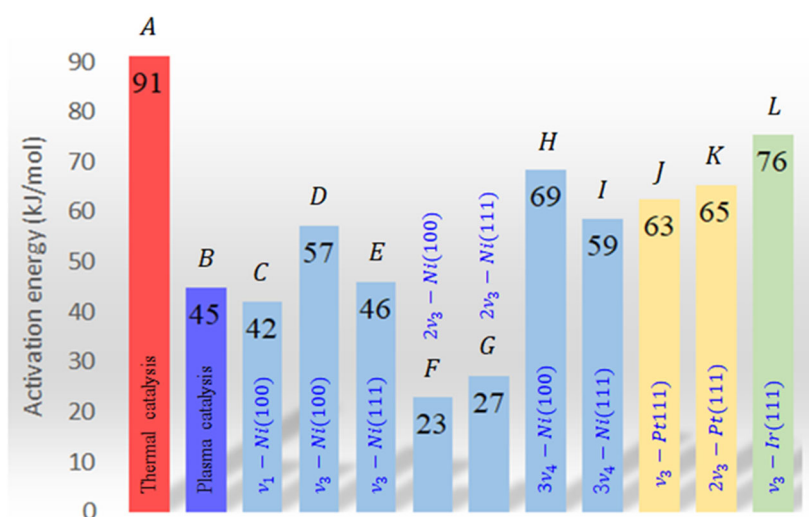


**Fig. 23.** Activation energy of vibrationally excited  $\text{CH}_4$  reacting over Ni [208]. With permission from Elsevier.

The activation energy was compared with the mode-selective vibrational kinetics of  $\text{CH}_4$  chemisorption over various Ni surfaces (Fig. 23). Unlike molecular beam studies, plasma catalysis possesses intrinsic complexity of phenomena: (1) the catalyst surface is not clean and is contaminated by various adsorbed species. (2) metal NPs inherently consist of various facets on their surfaces. Not only the metal surface, but also the support materials and catalyst-support-interfaces play a significant role. (3) Not all molecules are excited in the selective vibrational mode. Moreover, the radicals and charged particles play role. (4) Plasma-induced modification of crystal structure and/or crystal defects in metal oxide support materials are also important. Nevertheless, it is worth mentioning that the activation energy for selective vibrational  $\text{CH}_4$ , on average, is close to the experimentally observed activation energy. The results further indicate that the overtone stretching vibration mode ( $2\nu_3$ ) further decreases activation energy to 23–27  $\text{kJ mol}^{-1}$ . Although the overtone vibration mode is not generated by a single electron collision owing to the selection rule of vibrational transition, multiple electron collisions with vibrational species are possible when vibrational molecules are accumulated in a 100 kHz operation. The situation then becomes similar to the electron-induced ladder-climbing mechanism (see R1). Further reaction enhancement by DBD is highly anticipated.

#### 4.6 Modelling of plasma and catalyst: from each alone to in combination

Modeling of the plasma catalyst is an attempt to understand the five important matching issues described in Section 2.1 by combining plasma reactions, which are non-selective volumetric gaseous processes mostly at atmospheric pressure, and catalyst reactions, which are selective surface reaction at the gas-solid interface. Models for plasma include input variables, such as power supply, discharge gas, reactor geometry, and pellet type, and provide the spatial-temporal electric field, gas species density (even at a specific energy level), electron temperature, and gas temperature (including rotational and vibrational), which will eventually be important input data for atomic/molecular-scale simulation on the surface.

A typical plasma-catalyst reactor is a packed-bed concept, so the model must account for the complex geometry of packing materials to set up a calculation domain, and the pellets shapes can be spherical, spheroid, or even rod-shaped. Fig. 24 briefly describes the modeling approach used to obtain fundamental plasma parameters in plasma catalysis. Specific pellets coated with conductive/non-conductive catalytic materials can

be used; the surface pore structure, porosity, conductivity, and permittivity may be changed [31]. The boundary conditions of each electrode or pellet surface should be carefully determined. Assuming that the surface reaction model is important, the possible mechanisms are surface charging and charge accumulation, adsorption and desorption, recombination, secondary emissions, thermal reactions, and catalytic material-induced reactions. While the plasma-catalyst interactions seem complex, simulation can help us understand more with the power of simplicity by assuming a specific fluid or particle model.

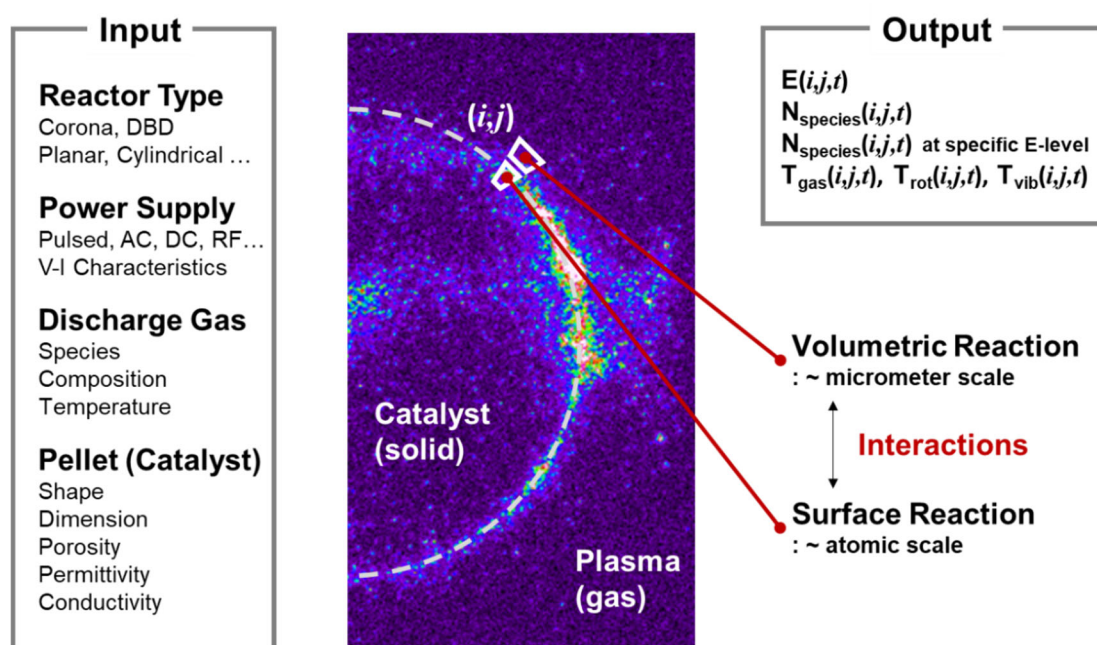


Fig. 24. Expected result of plasma catalyst modeling.

The fluid model approach is suitable for atmospheric plasma simulation at the micrometer scale [210–216]. Most of previous modeling studies have focused on analyzing the geometrical effects of packed materials. Kang *et al.* first attempted to simplify single and double-stacked packed-bed discharges in a 2-D fluid model and showed the advantage of a packed-bed structure that exhibits high electric field at the contact between neighboring pellets [210]. In the latter work, distinct streamer propagations on a spherical pellet surface without catalytic coating were discussed for primary/secondary streamer and cathode-directed streamer [212, 213]. Further studies have reported the concept of surface ionization wave [217], streamer propagation along the pellets and transfer to the void [215], and even interference of the metallic catalyst on the streamer propagation in 2-D models [214, 217]. Because the fluid model is advantageous for describing the classic multi-physics phenomena of plasma-catalyst, future simulation is expected to include more physical/chemical models to solve complex coupled phenomena such as material, chemical, and thermal effects. Although computing power is getting increased faster than ever, continuous efforts to optimize calculation algorithms are necessary to minimize the computation load and computing time. The quality of modeling results can be enhanced with proper feedback of measurement data, such as the gaseous/surface reaction cross-section, reaction rate, reaction path, and even information about the developing catalysts. Modeling of plasma dynamics on both the macro-scale (i.e., packed-bed reactor) and micro-scale including intrapores has been rapidly developing in recent years. Plasma modeling has been and will continue to be an attractive way to understand the physics of plasmas. It is believed that recent and future advances in plasma modeling continue to provide our society with valuable insights into plasma catalysis research.

Over the last two decades, computational science has become an essential tool in catalysis work to predict elementary reactions at the atomic/molecular scale and to determine the energy barrier and reaction pathways. Since catalytic reactions occur at the atomic level, the multi-dimensional phenomena of the gas (plasma) – solid (catalyst) reaction cannot be handled only by the fluid model. For this reason, recent studies have attempted particle or particle-fluid hybrid models and paid attention to atomic-scale simulations [218–221]. The flux- and species-resolved data from plasma modeling are imperative for atomic/molecular scale simulations to elucidate the true nature of plasma catalysis. The dynamic of atomic-scale interaction purely belong to the computational field, density function theory (DFT) calculation and molecular dynamics (MD),

because there is no available technology to monitor the rapid interaction between incident molecules and the surface with corresponding time resolution ( $10^{-12} \sim 10^{-10}$  s). There is no question about the importance of the roles of atomic-scale simulations in plasma catalysis. DFT calculations can provide the interatomic forces between hundreds of atoms and simulate detailed catalytic reactions; however, it is mostly static simulation for catalytic reactions within picoseconds. Previous work has shown that atomic-scale simulations can predict adsorption, chemical bond breakage, and diffusion into the atoms in a Ni catalyst under  $\text{CH}_x$  plasma [220]. DFT can also provide a more in-depth simulation of dry reforming and  $\text{CO}_2$  activation [218, 221]. Future simulation is expected to focus on the development of time-dependent DFT describing a longer reaction period including additional species in the calculation. Another challenge of atomic-scale simulation is to reduce the heavy computational load with less calculation time.

## 5. Conclusion

The publication trends of plasma catalysis clearly indicate the phase transition from early development to rapid growth. A variety of chemical reactions have been tested using different types of reactor designs, which sometimes makes it difficult to compare the results from one to another. This interim report outlines the past achievement in plasma catalysis and addresses some critical issues on which a general consensus needs to reach for further development. A special critique is given on the present state of plasma catalysis, especially regarding synergy.

As blueprints for future work, we have addressed several important issues and requirements. The development of *in situ* and *operando* measurement techniques is important for the systematic evaluation of plasma catalysis. The development of nanosecond pulsed power supply capable of delivering high voltage ( $\sim 30$  kV) with high frequency should be on the “To-Do list” for plasma community. Vibrational energy in plasma has long been considered a magic key for forthcoming big progress. We have addressed the promising possibility of incorporating vibrational energy by providing decent examples obtained from molecular beams and surface science. The development of new catalytic materials for  $\text{NH}_3$  synthesis also suggests another direction in which plasma catalysis can be pursued in the future. The combination of new materials and plasma still possesses immeasurable potential to open a new phase of the chemical reaction. Activity inversion indicates that a breakthrough in material matching can be achieved with unexpected materials that have been considered less active in conventional thermal catalysis. Atomic/molecular scale simulation combined with *operando* measurements is expected to answer important questions about the interfacial and defect control of catalytic reactions and the chemical nature of NPs.

We hope that this interim report can address some of the ongoing uncertainty and guide future development under intensive multidisciplinary collaborations between researchers from different scientific backgrounds.

## Acknowledgment

This work was supported by JST CREST (JPMJCR19R3) and JSPS KAKENHI Grant Number JP18H01208.

## References

- [1] Bogaerts, A., Tu, X., Whitehead, J. C., Centi, G., Lefferts, L., Guaitella, O., Azzolina-Jury, F., Kim, H.-H., Murphy, A. B., Schneider, W. F., Nozaki, T., Hicks, J. C., Rousseau, A., Thevenet, F., Khacef, A., and Carreon, M., The 2020 plasma catalysis roadmap, *J. Phys. D: Appl. Phys.*, Vol. 53 (44), pp. 443001, 2020.
- [2] Mizuno, A., Generation of non-thermal plasma combined with catalysts and their application in environmental technology, *Catal. Today*, Vol. 211, pp. 2–8, 2013.
- [3] Whitehead, J. C., Plasma-catalysis: the known knowns, the known unknowns and the unknown unknowns, *J. Phys. D: Appl. Phys.*, Vol. 49 (24), pp. 243001, 2016.
- [4] Neyts, E. C., Ostrikov, K., Sunkara, M. K., and Bogaerts, A., Plasma catalysis: Synergistic effects at the nanoscale, *Chem. Rev.*, Vol. 115, pp. 13408–13446, 2015.
- [5] Nozaki, T. and Okazaki, K., Non-thermal plasma catalysis of methane: Principles, energy efficiency, and applications, *Catal. Today*, Vol. 211, pp. 29–38, 2013.
- [6] Tu, X., Whitehead, J. C., and Nozaki, T., *Plasma Catalysis: Fundamentals and Applications*: Springer, 2019.

- [7] Kim, H. H., Tsunoda, K., Katsura, S., and Mizuno, A., A novel plasma reactor for NO<sub>x</sub> control using photocatalyst and hydrogen peroxide injection, *IEEE Trans. Ind. Applicat.*, Vol. 35 (6), pp. 1306–1310, 1999.
- [8] Oda, T., Kato, T., Takahashi, T., and Shimizu, K., Nitric oxide decomposition in air by using nonthermal plasma processing with additives and catalyst, *IEEE Trans. Ind. Applicat.*, Vol. 34 (2), pp. 268–271, 1998.
- [9] Hammer, T. and Broer, S., Plasma enhanced selective catalytic reduction of NO<sub>x</sub> in diesel exhaust; Test bench measurements, *Society of Automotive Engineers*, Vol., pp. Paper No. 1999-01-3633, 1999.
- [10] Marafee, A., Liu, C., Xu, G., Mallinson, R., and Lobban, L., An experimental study on the oxidative coupling of methane in a dielectric current corona discharge reactor over Sr/La<sub>2</sub>O<sub>3</sub> catalyst, *Ind. Eng. Chem. Res.*, Vol. 36, pp. 632–637, 1997.
- [11] Liu, C. J., Marafee, A., Mallinson, R., and Lobban, L., Methane conversion to higher hydrocarbons in a corona discharge over metal oxide catalyst with OH groups, *Appl. Catal. B: Environ.*, Vol. 164, pp. 21–33, 1997.
- [12] Eliasson, B., Kogelschatz, U., Xue, B., and Zhou, L., Hydrogenation of carbon dioxide to methane with a discharge-activated catalyst, *Ind. Eng. Chem. Res.*, Vol. 37, pp. 3350–3357, 1998.
- [13] Grinevich, V. I., Kolobova, N. V., and Kostrov, V. V., Influence of catalysts on sulfur dioxide and carbon monoxide oxidation in a barrier-discharge plasma, *High Energy Chem.*, Vol. 31 (6), pp. 400–403, 1997.
- [14] Sugiyama, K., Akazawa, K., Oshima, M., Miura, H., Matsuda, T., and Nomura, O., Ammonia synthesis by means of plasma over MgO catalyst, *Plasma Chem. Plasma Proc.*, Vol. 6 (2), pp. 179–193, 1986.
- [15] Sultana, S., Vandenbroucke, A. M., Leys, C., Geyter, N. D., and Morent, R., Abatement of VOCs with alternate adsorption and plasma-assisted regeneration: A review, *Catalysts*, Vol. 5, pp. 718–746, 2015.
- [16] Thevenet, F., Sivachandiran, L., Guaitella, O., Barakat, C., and Rousseau, A., Plasma-catalyst coupling for volatile organic compound removal and indoor air treatment: a review, *J. Phys. D: Appl. Phys.*, Vol. 47 (22), pp. 224011, 2014.
- [17] Djéga-Mariadassou, G., Baudin, F., Khacef, A., and Costa, P. D., "NO<sub>x</sub> Abatement by Plasma Catalysis," in *Plasma Chemistry and Catalysis in Gases and Liquids*, Lukes, P., Parvulescu, V. I., and Magureanu, M., Eds.: Wiley-VCH, pp. 89–129, 2012.
- [18] Tu, X., Gallon, H. J., Twigg, M. V., Gorry, P. A., and Whitehead, J. C., Dry reforming of methane over a Ni/Al<sub>2</sub>O<sub>3</sub> catalyst in a coaxial dielectric barrier discharge reactor, *J. Phys. D: Appl. Phys.*, Vol. 44 (27), pp. 274007, 2011.
- [19] Hong, J., Praver, S., and Murphy, A. B., Plasma catalysis as an alternative route for ammonia production: Status, mechanisms, and prospects for progress, *ACS Sustainable Chem. Eng.*, Vol. 6 (1), pp. 15–31, 2018.
- [20] Carreon, M. L., Plasma catalytic ammonia synthesis: state of the art and future directions, *J. Phys. D: Appl. Phys.*, Vol. 52 (48), pp. 483001, 2019.
- [21] Kim, H. H., Teramoto, Y., Ogata, A., Takagi, H., and Nanba, T., Plasma catalysis for environmental treatment and energy applications, *Plasma Chem. Plasma Proc.*, Vol. 36 (1), pp. 45–72, 2016.
- [22] Heberlein, J. and Murphy, A. B., Thermal plasma waste treatment, *J. Phys. D: Appl. Phys.*, Vol. 41 (5), pp. 053001, 2008.
- [23] Bal, K., Huygh, S., Bogaerts, A., and Neyts, E. C., Effect of plasma-induced surface charging on catalytic processes: application to CO<sub>2</sub> activation, *Plasma Sources Sci. Technol.*, Vol. 27 (2), pp. 024001, 2018.
- [24] Hyman, M. P. and Medlin, J. W., Theoretical study of the adsorption and dissociation of oxygen on Pt(111) in the presence of homogeneous electric fields, *J. Phys. Chem. B*, Vol. 109 (13), pp. 6304–6310.
- [25] Venugopalan, M. and Jones, R. A., Chemistry of dissociated water vapor and related systems, *Chem. Rev.*, Vol. 66, pp. 133–160, 1966.
- [26] White, H. J., *Industrial Electrostatic Precipitation*: Addison-Wesley Publishing Company, Inc., 1963.
- [27] White, H. J., Electrostatic precipitation of fly ash. Precipitator design, *J. Air Pollution Control Asso.*, Vol. 27 (3), pp. 206–217, 1977.
- [28] White, H. J., Electrostatic precipitation of fly ash. Precipitator equipment, precipitator case histories, *J. Air Pollution Control Asso.*, Vol. 27 (4), pp. 308–318, 1977.
- [29] Kim, H. H., Nonthermal plasma processing for air pollution control: A historical review, current issues, and future prospects, *Plasma Process. Polym.*, Vol. 1 (2), pp. 91–110, 2004.
- [30] Ono, R. and Tokuhiro, M., Spatiotemporal measurement of OH density from upstream to downstream in humid helium atmospheric-pressure plasma jet, *Plasma Source Sci. Technol.*, Vol. 29 (3), pp. 035021, 2020.
- [31] Kim, H. H., Teramoto, Y., Negishi, N., and Ogata, A., A multidisciplinary approach to understand the interactions of nonthermal plasma and catalyst: A review, *Catal. Today*, Vol. 256, pp. 13–22, 2015.
- [32] Huang, H. B., Ye, D. Q., Fu, M. L., and Feng, F. D., Contribution of UV light to the decomposition of toluene in dielectric barrier discharge plasma/photocatalysis system, *Plasma Chem. Plasma Proc.*, Vol. 27, pp. 577–588, 2007.
- [33] Maciucă, A., Batiot-Dupeyrat, C., and Tatibouet, J. M., Synergetic effect by coupling photocatalysis with plasma for low VOCs concentration removal from air, *Appl. Catal. B: Environ.*, Vol. 125, pp. 432–438, 2012.
- [34] Assadi, A. A., Bouzaza, A., Merabet, S., and Wolbert, D., Modeling and simulation of VOCs removal by nonthermal plasma discharge with photocatalysis in a continuous reactor: Synergetic effect and mass transfer, *Chem. Eng. Journal*, Vol. 258, pp. 119–127, 2014.

- [35] Sheng, Z., Kameshima, S., Yao, S., and Nozaki, T., Oxidation behavior of Ni/Al<sub>2</sub>O<sub>3</sub> catalyst in nonthermal plasma-enabled catalysis, *J. Phys. D: Appl. Phys.*, Vol. 51, pp. 445205, 2018.
- [36] Einaga, H. and Ogata, A., Benzene oxidation with ozone over supported manganese oxide catalysts: Effect of catalyst support and reaction conditions, *J. Hazard. Materials*, Vol. 164, pp. 1236–1241, 2009.
- [37] Ogata, A., Saito, K., Kim, H. H., Sugawara, M., Aritani, H., and Einaga, H., Performance of an ozone decomposition catalyst in hybrid plasma reactors for volatile organic compound removal, *Plasma Chem. Plasma Proc.*, Vol. 30, pp. 33–42, 2010.
- [38] Ghorbani, M., Omraei, M., Jafari, M., and Katal, R., Application of different catalysts for oxidation of toluene in absence and presence of ozone, *Asian J. Chem.*, Vol. 22 (10), pp. 8179–8184, 2010.
- [39] Somorjai, G. A., The experimental evidence of the role of surface restructuring during catalytic reactions *Catal. Lett.*, Vol. 12 (1–3), pp. 17–34, 1992.
- [40] Bal, K. M. and Neyts, E. C., Merging metadynamics into hyperdynamics: accelerated molecular simulations reaching time scales from microseconds to seconds, *J. Chem. Theory Comput.*, Vol. 11, pp. 4545–4554, 2015.
- [41] Kim, H. H., Ogata, A., Schiorlin, M., Marotta, E., and Paradisi, C., Oxygen isotope (<sup>18</sup>O<sub>2</sub>) evidence on the role of oxygen in the plasma-driven catalysis of VOC oxidation, *Catal. Lett.*, Vol. 141 (2), pp. 277–282, 2011.
- [42] Guaitella, O., Lazzaroni, C., Marinov, D., and Rousseau, A., Evidence of atomic adsorption on TiO<sub>2</sub> under plasma exposure and related C<sub>2</sub>H<sub>2</sub> surface reactivity, *Appl. Phys. Lett.*, Vol. 97, pp. 011502, 2010.
- [43] Guaitella, O., Hubner, M., Welzel, S., Marinov, D., Ropecke, J., and Rousseau, A., Evidence for surface oxidation on pyrex of NO into NO<sub>2</sub> by adsorbed O atoms, *Plasma Sources Sci. Technol.*, Vol. 19, pp. 045206, 2010.
- [44] Marinov, D., Guaitella, O., Booth, J. P., and Rousseau, A., Direct observation of ozone formation on SiO<sub>2</sub> surfaces in O<sub>2</sub> discharges, *J. Phys. D: Appl. Phys.*, Vol. 46 (3), pp. 032001, 2013.
- [45] Marinov, D., Guaitella, O., Arcos, T. d. I., Keudell, A. v., and Rousseau, A., Adsorption and reactivity of nitrogen atoms on silica surface under plasma exposure, *J. Phys. D: Appl. Phys.*, Vol. 47 (47), pp. 475204, 2014.
- [46] Marinov, D., Lopatik, D., Guaitella, O., Ionikh, Y., Ropecke, J., and Rousseau, A., Surface deactivation of vibrationally excited N<sub>2</sub> studied using infrared titration combined with quantum cascade laser absorption spectroscopy, *J. Phys. D: Appl. Phys.*, Vol. 47 (1), pp. 015203, 2014.
- [47] Teramoto, Y., Kim, H. H., Ogata, A., and Negishi, N., Study of plasma-induced surface active oxygen on zeolite-supported silver nanoparticles, *Catal. Lett.*, Vol. 143, pp. 1374–1378, 2013.
- [48] Mangolini, L. and Kortshagen, U., Selective nanoparticle heating: Another form of nonequilibrium in dusty plasmas, *Phys. Rev. E*, Vol. 79, pp. 026405, 2009.
- [49] Kramer, N. J., Anthony, R. J., Mamunuru, M., Aydil, E. S., and Kortshagen, U. R., Plasma-induced crystallization of silicon nanoparticles, *J. Phys. D: Appl. Phys.*, Vol. 47 (7), pp. 075202, 2014.
- [50] Wolter, M., Levchenko, I., Kersten, H., and Ostrikov, K., Hydrogen in plasma-nanofabrication: Selective control of nanostructure heating and passivation, *Appl. Phys. Lett.*, Vol. 96 (13), pp. 133105, 2010.
- [51] Biener, J., Wittstock, A., Zepeda-Ruiz, L. A., Biener, M. M., Zielasek, V., Kramer, D., Viswanath, R. N., J. Weissmüller, B. Bäumer, M., and Hamza, A. V., Surface-chemistry-driven actuation in nanoporous gold, *Nat. Mater.*, Vol. 8, pp. 47–51, 2009.
- [52] Wittstock, A. and Bäumer, M., Catalysis by unsupported skeletal gold catalysts, *Acc. Chem. Res.*, Vol. 47 (3), pp. 731–739, 2014.
- [53] Kusada, K., Kobayashi, H., Ikeda, R., Kubota, Y., Takata, M., Toh, S., Yamamoto, T., Matsumura, S., Sumi, N., Sato, K., Nagaoka, K., and Kitagawa, H., Solid solution alloy nanoparticles of immiscible Pd and Ru elements neighboring on Rh: Changeover of the thermodynamic behavior for hydrogen storage and enhanced CO-oxidizing ability, *J. Am. Chem. Soc.*, Vol. 136 (5), pp. 1864–1871, 2014.
- [54] Tou, A., Kim, H. H., Einaga, H., Teramoto, Y., and Ogata, A., Ozone-assisted catalysis of CO: In situ Fourier transform IR evidence of the cooperative effect of a bimetallic Ag–Pd catalyst, *Chem. Eng. J.*, Vol. 355, pp. 380–389, 2019.
- [55] Huang, D. C., Chang, K. H., Pong, W. F., Tseng, P. K., Hung, K. J., and Huang, W. F., Effect of Ag-promotion on Pd catalysts by XANES, *Catal. Lett.*, Vol. 53, pp. 155–159, 1998.
- [56] Jidenko, N., Bourgeois, E., and Borra, J. P., Temperature profiles in filamentary dielectric barrier discharges at atmospheric pressure, *J. Phys. D: Appl. Phys.*, Vol. 43 (29), pp. 295203, 2010.
- [57] Anghel, S. D., Generation and electrical diagnostic of an atmospheric-pressure dielectric barrier discharge, *IEEE Trans. Plasma Sci.*, Vol. 39 (3), pp. 871–876, 2011.
- [58] Li, J., Bai, S. P., Shi, X. C., Han, S. L., Zhu, X. M., Chen, W. C., and Pu, Y. K., Effects of temperature on benzene oxidation in dielectric barrier discharges, *Plasma Chem. Plasma Proc.*, Vol. 28, pp. 39–48, 2008.
- [59] Kameshima, S., Mizukami, R., Yamazaki, T., Prananto, L. A., and Nozaki, T., Interfacial reactions between DBD and porous catalyst in dry methane reforming, *J. Phys. D: Appl. Phys.*, Vol. 51 (11), pp. 114006, 2018.
- [60] Nozaki, T., Miyazaki, Y., Unno, Y., and Okazaki, K., Energy distribution and heat transfer mechanisms in atmospheric pressure non-equilibrium plasmas, *J. Phys. D: Appl. Phys.*, Vol. 34, pp. 3383–3390, 2001.
- [61] Nozaki, T., Unno, Y., and Okazaki, K., Thermal structure of atmospheric pressure non-equilibrium plasma, *Plasma Source Sci. Technol.*, Vol. 11 (4), pp. 431–438, 2002.

- [62] Kim, H. H., Teramoto, Y., and Ogata, A., Time-resolved imaging of positive pulsed corona-induced surface streamers on TiO<sub>2</sub> and  $\gamma$ -Al<sub>2</sub>O<sub>3</sub>-supported Ag catalysts, *J. Phys. D: Appl. Phys.*, Vol. 49 (41), pp. 415204, 2016.
- [63] Du, Y., Tamura, K., Moore, S., Peng, Z., Nozaki, T., and Bruggeman, P. J., CO(B<sup>1</sup> $\Sigma^+$   $\rightarrow$  A<sup>1</sup> $\Pi$ ) angstrom system for gas temperature measurements in CO<sub>2</sub> containing plasmas, *Plasma Chem. Plasma Proc.*, Vol. 37, pp. 29–41, 2017.
- [64] Nozaki, T., Abe, S., Moriyama, S., Kameshima, S., Okazaki, K., Goujard, V., and Agiral, A., One step methane conversion to syngas by dielectric barrier discharge, *Jpn. J. Appl. Phys.*, Vol. 54 (1S), pp. 01AG01, 2014.
- [65] Nie, Q. Y., Cao, Z., Ren, C. S., Wang, D. Z., and Kong, M. G., A two-dimensional cold atmospheric plasma jet array for uniform treatment of large-area surfaces for plasma medicine, *New J. Phys.*, Vol. 11, pp. 115015, 2009.
- [66] Parastaev, A., Hoeben, W. F. L. M., Heesch, B. E. J. M. v., Kosinov, N., and Hensen, E. J. M., Temperature-programmed plasma surface reaction: An approach to determine plasma-catalytic performance, *Appl. Catal. B: Environ.*, Vol. 239, pp. 168–177, 2018.
- [67] Nozaki, T., Hiroyuki, T., and Okazaki, K., Hydrogen enrichment of low-calorific fuels using barrier discharge enhanced Ni/ $\gamma$ -Al<sub>2</sub>O<sub>3</sub> bed reactor: Thermal and nonthermal effect of nonequilibrium plasma, *Energy & Fuel*, Vol. 21 (1), pp. 339–345, 2006.
- [68] Mizuno, A. and Ito, H., Basic performance of an electrostatically augmented filter consisting of a packed ferroelectric pellet layer, *J. Electrostat.*, Vol. 25, pp. 97–107, 1990.
- [69] Mizuno, A. and Ito, H., "An electrostatic precipitator using a ferroelectric pellet layer for particle collection," presented at IEEE IAS Annual Meeting, 1986.
- [70] Mizuno, A., Yamazaki, Y., Ito, H., and Yoshida, H., ac energized ferroelectric pellet bed gas cleaner, *IEEE Trans. Ind. Applicat.*, Vol. 28 (3), pp. 535–540, 1992.
- [71] Yoshida, H., Marui, Z., Aoyama, M., Sugiura, J., and Mizuno, A., Removal of odor gas component utilizing plasma chemical reactions promoted by the partial discharge in a ferroelectric pellet layer, *J. Inst. Electrostat. Jpn.*, Vol. 13 (5), pp. 425–430, 1989 (in Japanese).
- [72] Yamamoto, T., Ramanathan, K., Lawless, P. L., Ensor, D. S., Newsome, J. R., Plaks, N., and Ramsey, G. H., Control of volatile organic compounds by an ac energized ferroelectric pellet reactor and a pulsed corona reactor, *IEEE Trans. Ind. Applicat.*, Vol. 28 (3), pp. 528–534, 1992.
- [73] Nunez, C. M., Ramsey, G. H., Ponder, W. H., Abbott, J. H., Hamel, L. E., and Kariher, P. H., Corona destruction: An innovative control technology for VOCs and air toxics, *J. Air & Waste Manage. Assoc.*, Vol. 42, pp. 242–247, 1993.
- [74] Tonkyn, R. G., Barlow, S. E., and Orlando, T. M., Destruction of carbon tetrachloride in a dielectric barrier/packed-bed corona reactor, *J. Appl. Phys.*, Vol. 80 (9), pp. 4877–4886, 1996.
- [75] Ogata, A., Yamanouchi, K., Mizuno, K., Kushiyama, S., and Yamamoto, T., Decomposition of benzene using alumina-hybrid and catalyst-hybrid plasma reactors, *IEEE Trans. Ind. Applicat.*, Vol. 35 (6), pp. 1289–1295, 1999.
- [76] Ogata, A., Yamanouchi, K., Mizuno, K., Kushiyama, S., and Yamamoto, T., Oxidation of dilute benzene in an alumina hybrid plasma reactor at atmospheric pressure, *Plasma Chem. Plasma Proc.*, Vol. 19 (3), pp. 383–394, 1999.
- [77] Mizuno, A., Yamazaki, Y., Obama, S., Suzuki, E., and Okazaki, K., Effect of voltage waveform on partial discharge in ferroelectric pellet layer for gas cleaning, *IEEE Trans. Ind. Applicat.*, Vol. 29 (2), pp. 262–267, 1993.
- [78] Kim, H. H., Teramoto, Y., Sano, T., Negishi, N., and Ogata, A., Effects of Si/Al ratio on the interaction of nonthermal plasma and Ag/HY catalysts, *Appl. Catal. B: Environ.*, Vol. 166–167, pp. 9–17, 2015.
- [79] Wang, W., Kim, H. H., Laer, K. V., and Bogaerts, A., Streamer propagation in a packed bed plasma reactor for plasma catalysis applications, *Chem. Eng. Journal*, Vol. 334, pp. 2467–2479, 2018.
- [80] Patil, B., Cherkasov, N., Lang, J., Ibhaddon, A., Hessel, V., and Wang, Q., Low temperature plasmacatalytic NO<sub>x</sub> synthesis in a packed DBD reactor: Effect of support materials and supported active metal oxides, *Appl. Catal. B: Environ.*, Vol. 194, pp. 123–133, 2016.
- [81] Anderegg, F. O., Surface complications in the corona discharge, *Trans. Am. Electrochemical Soc.*, Vol. 44, pp. 203–214, 1923.
- [82] Anderegg, F. O. and Herr, W. N., The formation of active hydrogen in the creepage corona discharge, *J. Am. Chem. Soc.*, Vol. 47 (10), pp. 2429–2431, 1925.
- [83] Gallon, H., Kim, H. H., Tu, X., and Whitehead, J. C., Microscope-ICCD imaging of an atmospheric pressure CH<sub>4</sub> and CO<sub>2</sub> dielectric barrier-discharge, *IEEE Trans. Plasma Sci.*, Vol. 39 (11), pp. 2176–2177, 2011.
- [84] Schmidt-Szalowski, K. and Borucka, A., Heterogeneous effect in the process of ozone synthesis in electrical discharges, *Plasma Chem. Plasma Proc.*, Vol. 9 (2), pp. 235–255, 1989.
- [85] Song, Y. H., Kim, S. J., Choi, K. I., and Yamamoto, T., Effects of adsorption and temperature on a nonthermal plasma process for removing VOCs, *J. Electrostat.*, Vol. 55, pp. 189–201, 2002.
- [86] Ogata, A., Ito, D., Mizuno, K., Kushiyama, S., and Yamamoto, T., Removal of dilute benzene using a zeolite-hybrid plasma reactor, *IEEE Trans. Ind. Applicat.*, Vol. 37 (4), pp. 959–964, 2001.
- [87] Ogata, A., Ito, D., Mizuno, K., Kushiyama, S., Gal, A., and Yamamoto, T., Effect of coexisting components on aromatic decomposition in a packed-bed plasma reactor, *Appl. Catal. A: Gen.*, Vol. 236, pp. 9–15, 2002.
- [88] Kim, H. H. and Ogata, A., Interaction of nonthermal plasma with catalyst for the air pollution control, *Int. J. Plasma Environ. Sci. Technol.*, Vol. 6 (1), pp. 43–48, 2012.

- [89] Yamamoto, T., Optimization of nonthermal plasma for the treatment of gas streams, *J. Hazard. Materials*, Vol. B67, pp. 165–181, 1999.
- [90] Kang, W. S., Lee, D. H., Lee, J. O., Hur, M., and Song, Y. H., Combination of plasma with a honeycomb-structured catalyst for automobile exhaust treatment, *Environ. Sci. Technol.*, Vol. 47, pp. 11358–11362, 2013.
- [91] Nguyen, D. B., Shirjana, S., Hossain, M. M., Heo, I., and Mok, Y. S., Effective generation of atmospheric pressure plasma in a sandwich-type honeycomb monolith reactor by humidity control, *Chem. Eng. J.*, Vol. 401, pp. 125970, 2020.
- [92] Jansky, J., Tholin, F., Bonaventura, Z., and Bourdon, A., Simulation of the discharge propagation in a capillary tube in air at atmospheric pressure, *J. Phys. D: Appl. Phys.*, Vol. 43 (39), pp. 395201, 2010.
- [93] Jansky, J., Delliou, P. L., Tholin, F., Tardiveau, P., Bourdon, A., and Pasquiers, S., Experimental and numerical study of the propagation of a discharge in a capillary tube in air at atmospheric pressure, *J. Phys. D: Appl. Phys.*, Vol. 44 (33), pp. 335201, 2011.
- [94] Blin-Simiand, N., Tardiveau, P., Risacher, A., Jorand, F., and Pasquiers, S., Removal of 2-heptanone by dielectric barrier discharges - The effect of a catalyst support, *Plasma Process. Polym.*, Vol. 2 (3), pp. 256–262, 2005.
- [95] Rajanikanth, S., Kumar, P. K. S., and Ravi, V., Non-conventional plasma assisted catalysts for diesel exhaust treatment: A case study, *Plasma Sci. Technol.*, Vol. 4 (1), pp. 1119–1126, 2002.
- [96] Kuroki, T., Fujioka, T., Okubo, M., and Yamamoto, T., Toluene concentration using honeycomb nonthermal plasma desorption, *Thin Solid Films*, Vol. 515, pp. 4272–4277, 2007.
- [97] Kuroki, T., Fujioka, T., Kawabata, R., Okubo, M., and Yamamoto, T., Regeneration of honeycomb zeolite by nonthermal plasma desorption of toluene, *IEEE Trans. Ind. Appl.*, Vol. 45 (1), pp. 10–15, 2009.
- [98] Shimizu, K., Hirano, T., and Oda, T., Effect of water vapor and hydrocarbons in removing NO<sub>x</sub> by using nonthermal plasma and catalyst, *IEEE Trans. Ind. Appl.*, Vol. 37 (2), pp. 464–471, 2001.
- [99] Kim, H. H., Application of non-thermal plasma in environmental protection, Ph.D Thesis, Toyohashi University of Technology, 2000.
- [100] Oda, T., Takahashi, T., and Kohzuma, S., Decomposition of dilute trichloroethylene by using non-thermal plasma processing-frequency and catalyst effect, *IEEE Trans. Ind. Appl.*, Vol. 37 (4), pp. 965–970, 2001.
- [101] Feng, F., Zheng, Y., Shen, X., Zheng, Q., Dai, S., Zhang, X., Huang, Y., Liu, Z., and Yan, K., Characteristics of back corona discharge in a honeycomb catalyst and its application for treatment of volatile organic compounds, *Environ. Sci. Technol.*, Vol. 49, pp. 6831–6837, 2015.
- [102] Saud, S., Nguyen, D. B., Bhattarai, R. M., Matyakubov, N., Heo, I., Kim, S. J., Kim, Y. J., Lee, J. H., and Mok, Y. S., Dependence of humidified air plasma discharge performance in commercial honeycomb monoliths on the configuration and key parameters of the reactor, *J. Hazard. Materials*, Vol. 404, pp. 124024, 2021.
- [103] Hossain, M. M., Mo, Y. S., Nguyen, D. B., Kim, S.-J., Kim, Y. J., Lee, J. H., and Heo, I., Nonthermal plasma in practical-scale honeycomb catalysts for the removal of toluene, *J. Hazard. Materials*, Vol. 404, pp. 123958, 2021.
- [104] Okubo, M., Arita, N., Kuroki, T., and Yamamoto, T., Carbon particulate matter incineration in diesel engine emissions using indirect nonthermal plasma processing, *Thin Solid Films*, Vol. 515, pp. 4289–4295, 2007.
- [105] Hensel, K. and Tardiveau, P., ICCD camera imaging of discharges in porous ceramics, *IEEE Trans. Plasma Sci.*, Vol. 36 (4), pp. 980–981, 2008.
- [106] Sato, S., Hensel, K., Hayashi, H., Takashima, K., and Mizuno, A., Honeycomb discharge for diesel exhaust cleaning, *J. Electrostat.*, Vol. 67 (2–3), pp. 77–83, 2009.
- [107] Hensel, K., Microdischarges in ceramic foams and honeycombs, *Eur. Phys. J. D*, Vol. 54, pp. 141–148, 2009.
- [108] Takashima, K., Suzuki, T., Nomura, Y., Hinata, Y., Hayashi, H., Kurita, H., and Mizuno, A., Honeycomb discharge generated with a single high voltage power supply for activating catalyst, *Int. J. Plasma Environ. Sci. Technol.*, Vol. 7 (2), pp. 142–147, 2013.
- [109] Sato, S. and Mizuno, A., NO<sub>x</sub> removal of simulated diesel exhaust with honeycomb discharge, *Int. J. Plasma Environ. Sci. Technol.*, Vol. 4 (1), pp. 18–23, 2010.
- [110] Cimerman, R. and Hensel, K., Generation of honeycomb discharge assisted by micro-hollow surface dielectric barrier discharge, *Int. J. Plasma Environ. Sci. Technol.*, Vol. 15, pp. e01003, 2021.
- [111] Graupner, K., Binner, J., Fox, N., Garner, C. P., Harry, J. E., Hoare, D., Ladha, K. S., Mason, A., and Williams, A. M., Pulsed discharge regeneration of diesel particulate filters, *Plasma Chem. Plasma Proc.*, Vol. 33, pp. 467–477, 2013.
- [112] Zhang, Q.-Z. and Bogaerts, A., Plasma streamer propagation in structured catalysts, *Plasma Source Sci. Technol.*, Vol. 27 (10), pp. 105013, 2018.
- [113] Hensel, K., Sato, S., and Mizuno, A., Sliding discharge inside glass capillaries, *IEEE Trans. Plasma Sci.*, Vol. 36 (4), pp. 1282–1283, 2008.
- [114] Nguyen, D. B., Saud, S., Matyakubov, N., Mok, Y. S., Ryu, S., Jeon, H., and Kim, S. B., Propagation of humidified air plasma in a sandwich-type honeycomb plasma reactor and its dependence on the ambient temperature and reactor diameter, *Plasma Source Sci. Technol.*, Vol. 29 (12), pp. 125016, 2020.
- [115] Falkenstein, Z. and Coogan, J. J., Microdischarge behaviour in the silent discharge of nitrogen-oxygen and water-air mixtures, *J. Phys. D: Appl. Phys.*, Vol. 30, pp. 817–825, 1997.

- [116] Busse, C., Freund, H., and Schwieger, W., Intensification of heat transfer in catalytic reactors by additively manufactured periodic open cellular structures (POCS), *Chem. Eng. Process: Process Intensification*, Vol. 124, pp. 199–214, 2018.
- [117] Lee, H. and Sekiguchi, H., Plasma-catalytic hybrid system using spouted bed with a gliding arc discharge: CH<sub>4</sub> reforming as a model reaction, *J. Phys. D: Appl. Phys.*, Vol. 44 (27), pp. 274008, 2011.
- [118] Wang, Q., Cheng, Y., and Jin, Y., Dry reforming of methane in an atmospheric pressure plasma fluidized bed with Ni/γ-Al<sub>2</sub>O<sub>3</sub> catalyst, *Catal. Today*, Vol. 148 (3-4), pp. 275–282, 2009.
- [119] Bouchoul, N., Touati, H., ElodieFourré, Clacens, J.-M., and Batiot-Dupeyrat, C., Efficient plasma-catalysis coupling for CH<sub>4</sub> and CO<sub>2</sub> transformation in a fluidized bed reactor: Comparison with a fixed bed reactor, *Fuel*, Vol. 288, pp. 119575, 2021.
- [120] Lee, D. H., Song, Y.-H., Kim, K.-T., Jo, S., and Kang, H., Current state and perspectives of plasma applications for catalyst regeneration, *Catal. Today*, Vol. 337, pp. 15–27, 2019.
- [121] Kim, H. H., Tsubota, S., Daté, M., Ogata, A., and Futamura, S., Catalyst regeneration and activity enhancement of Au/TiO<sub>2</sub> by atmospheric pressure nonthermal plasma, *Appl. Catal. A: Gen.*, Vol. 329, pp. 93–98, 2007.
- [122] Kim, T., Lee, D. H., Jo, S. K., Pyun, S. H., Kim, K. T., and Song, Y. H., Mechanism of the accelerated reduction of an oxidized metal catalyst under electric discharge, *ChemCatChem*, Vol. 8, pp. 685–689, 2016.
- [123] Lee, D. H., Kim, H., Song, Y. H., and Kim, K. T., Plasma burner for active regeneration of diesel particulate filter, *Plasma Chem. Plasma Proc.*, Vol. 34, pp. 159–173, 2014.
- [124] Wang, T. and Schmidt, L. D., Intraparticle redispersion of Rh and Pt-Rh particles on SiO<sub>2</sub> and Al<sub>2</sub>O<sub>3</sub> by oxidation-reduction cycling, *J. Catal.*, Vol. 70, pp. 187–197, 1981.
- [125] Weststrate, C. J., Hauman, M. M., Moodley, D. J., Saib, A. M., Steen, E. v., and Niemantsverdriet, J. W., Cobalt fischer-tropsch catalyst regeneration: The crucial role of the kirkendall effect for cobalt redispersion, *Top. Catal.*, Vol. 54, pp. 811–816, 2011.
- [126] Balcerzaka, J., Redzynia, W., and Tyczkowski, J., In-situ XPS analysis of oxidized and reduced plasma deposited ruthenium-based thin catalytic films, *Appl. Surf. Sci.*, Vol. 426, pp. 852–855, 2017.
- [127] Bonanni, S., Ait-Mansour, K., Brune, H., and Harbich, W., Overcoming the strong metal-support interaction state: Co oxidation on TiO<sub>2</sub>(110)-supported Pt nanoclusters, *Acs Catalysis*, Vol. 1, pp. 385–389, 2011.
- [128] Bell, A. T., The impact of nanoscience on heterogeneous catalysis, *Science*, Vol. 299, pp. 1688–1691, 2003.
- [129] Finney, E. E. and Finke, R. G., Catalyst sintering kinetics data: Is there a minimal chemical mechanism underlying kinetics previously fit by empirical powerlaw expressions - and if so, what are its implications?, *Ind. Eng. Chem. Res.*, Vol. 56, pp. 10271–10286, 2017.
- [130] Hansen, T. W., Delariva, A. T., Challa, S. R., and Datye, A. K., Sintering of catalytic nanoparticles: Particle migration or Ostwald ripening?, *Acc. Chem. Res.*, Vol. 46 (8), pp. 1720–1730, 2013.
- [131] Nishihata, Y., Mizuki, J., Akao, T., Tanaka, H., Uenishi, M., Kimura, M., Okamoto, T., and Hamada, N., Self-regeneration of a Pd-perovskite catalyst for automotive emissions control, *Nature*, Vol. 418, pp. 164–167, 2002.
- [132] Yoshida, H., Omote, H., and Takeda, S., Oxidation and reduction processes of platinum nanoparticles observed at the atomic scale by environmental transmission electron microscopy, *Nanoscale*, Vol. 6, pp. 13113–13118, 2014.
- [133] Kamiuchi, N., Sun, K., Aso, R., Tane, M., Tamaoka, T., Yoshida, H., and Takeda, S., Self-activated surface dynamics in gold catalysts under reaction environments, *Nature Commun.*, Vol. 9, pp. 2060, 2018.
- [134] Yoshida, H., Kuwauchi, Y., Jinschek, J. R., Sun, K., Tanaka, S., Kohyama, M., Shimada, S., Haruta, M., and Takeda, S., Visualizing gas molecules interacting with supported nanoparticulate catalysts at reaction conditions, *Science*, Vol. 335, pp. 317–320, 2012.
- [135] Jwa, E., Lee, S. B., Lee, H. W., and Mok, Y. S., Plasma-assisted catalytic methanation of CO and CO<sub>2</sub> over Ni-zeolite catalysts, *Fuel Process. Technol.*, Vol. 108, pp. 89–93, 2013.
- [136] Wang, Z., Zhang, Y., Neyts, E. C., Cao, X., Zhang, X., Jang, B. W.-L., and Liu, C. J., Catalyst preparation with plasmas: How does it work?, *ACS Catalysis*, Vol. 8, pp. 2093–2110, 2018.
- [137] Witvrouwen, T., Paulussen, S., and Sels, B., The use of non-equilibrium plasmas for the synthesis of heterogeneous catalysts, *Plasma Process. Polym.*, Vol. 9, pp. 750–759, 2012.
- [138] Liu, X., Mou, C. Y., Lee, S., Li, Y., Secrest, J., and Jang, B. W. L., Room temperature O<sub>2</sub> plasma treatment of SiO<sub>2</sub> supported Au catalysts for selective hydrogenation of acetylene in the presence of large excess of ethylene, *J. Catal.*, Vol. 285, pp. 152–159, 2012.
- [139] Zhang, C., Jiang, L., Zhang, Y., Hu, J., and Leung, M. K. H., Janus effect of O<sub>2</sub> plasma modification on the electrocatalytic hydrogen evolution reaction of MoS<sub>2</sub>, *J. Catal.*, Vol. 361, pp. 384–392, 2018.
- [140] Di, L., Li, Z., Park, D.-W., Lee, B., and Zhang, X., Atmospheric-pressure cold plasma for synthesizing Pd/FeOx catalysts with enhanced low-temperature CO oxidation activity, *Jpn. J. Appl. Phys.*, Vol. 56, pp. 060301, 2017.
- [141] Pastor-Pérez, L., Belda-Alcázar, V., Marini, C., Pastor-Blas, M. M., Sepúlveda-Escribano, A., and Ramos-Fernandez, E. V., Effect of cold Ar plasma treatment on the catalytic performance of Pt/CeO<sub>2</sub> in water-gas shift reaction (WGS), *Appl. Catal. B: Environ.*, Vol. 225, pp. 121–127, 2018.
- [142] Blecha, J., Dudas, J., Lodes, A., and Derco, J., Activation of tungsten oxide catalyst on SiO<sub>2</sub> surface by low-temperature plasma, *J. Catal.*, Vol. 116 (1), pp. 285–290, 1989.

- [143] Liu, C.J., Yu, K., Zhang, Y.P., Zhu, X., He, F., and Eliasson, B., Remarkable improvement in the activity and stability of Pd/HZSM-5 catalyst for methane combustion, *Catal. Commun.*, Vol. 4 (7), pp. 303–307, 2003.
- [144] Zhang, Y.-P., Ma, P.-S., Zhu, X., Liu, C.-J., and Shen, Y., A novel plasma-treated Pt/NaZSM-5 catalyst for NO reduction by methane, *Catal. Commun.*, Vol. 5, pp. 35–39, 2004.
- [145] Jin, L., Qian, K., Jiang, Z., and Huang, W., Ag/SiO<sub>2</sub> catalysts prepared via  $\gamma$ -ray irradiation and their catalytic activities in CO oxidation, *J. Mol. Catal. A: Chemical*, Vol. 274, pp. 95–100, 2007.
- [146] Menard, L. D., Xu, F., Nuzzo, R. G., and Yang, J. C., Preparation of TiO<sub>2</sub>-supported Au nanoparticle catalysts from a Au<sub>13</sub> cluster precursor: Ligand removal using ozone exposure versus a rapid thermal treatment, *J. Catal.*, Vol. 243, pp. 64–73, 2006.
- [147] Wang, B., Chen, B., Sun, Y., Xiao, H., Xu, X., Fua, M., Wu, J., Chen, L., and Ye, D., Effects of dielectric barrier discharge plasma on the catalytic activity of Pt/CeO<sub>2</sub> catalysts, *Appl. Catal. B: Environ.*, Vol. 238, pp. 328–338, 2018.
- [148] Zou, J. J., He, H., Cui, L., and Du, H. Y., Highly efficient Pt/TiO<sub>2</sub> photocatalyst for hydrogen generation prepared by a cold plasma method, *Int. J. Hydrogen Energy*, Vol. 32, pp. 1762–1770, 2007.
- [149] Xu, H., Luo, J., and Chu, W., Non-thermal plasma-treated gold catalyst for CO oxidation, *RSC Advances*, Vol. 4, pp. 25729–25735, 2014.
- [150] Wang, Z., Li, Q.-K., Zhang, C., Cheng, Z., Chen, W., McHugh, E. A., Carter, R. A., Yakobson, B. I., and Tour, J. M., Hydrogen peroxide generation with 100% Faradaic efficiency on metal-free carbon black, *ACS Catalysis*, Vol. 11 (2454–2459), pp. 2021.
- [151] Zhang, S., Li, X.-S., Zhu, B., Liu, J.-L., Zhu, X., Zhu, A.-M., and Jang, B. W.-L., Atmospheric-pressure O<sub>2</sub> plasma treatment of Au/TiO<sub>2</sub> catalysts for CO oxidation, *Catal. Today*, Vol. 256, pp. 142–147, 2015.
- [152] Di, L., Zhang, X., Xu, Z., and Wang, K., Atmospheric-pressure cold plasma for preparation of high performance Pt/TiO<sub>2</sub> photocatalyst and its mechanism, *Plasma Chem. Plasma Proc.*, Vol. 34, pp. 301–311, 2014.
- [153] Yu, K. L., Liu, C. J., Zhang, Y. P., He, F., Zhu, X. L., and Eliasson, B., The preparation and characterization of highly dispersed PdO over alumina for low-temperature combustion of methane, *Plasma Chem. Plasma Proc.*, Vol. 24 (3), pp. 393–403, 2004.
- [154] Yang, X., Zhao, F., Yeh, Y. W., Selinsky, R. S., Chen, Z., Yao, N., Tully, C. G., Ju, Y., and Koel, B. E., Nitrogen-plasma treated hafnium oxyhydroxide as an efficient acid-stable electrocatalyst for hydrogen evolution and oxidation reactions, *Nature Commun.*, Vol. 10, pp. 1543, 2019.
- [155] Chu, W., Wang, L. N., Chernavskii, P. A., and Khodakov, A. Y., Glow-discharge plasma-assisted design of cobalt catalysts for Fischer-Tropsch synthesis, *Angew. Chem. Int. Ed.*, Vol. 47, pp. 5052–5055, 2008.
- [156] Zou, J. J., Zhang, Y. P., and Liu, C. J., Reduction of supported noble-metal ions using glow discharge plasma, *Langmuir*, Vol. 22 (26), pp. 11388–11394, 2006.
- [157] Yan, X., Zhao, B., Liu, Y., and Li, Y., Dielectric barrier discharge plasma for preparation of Ni-based catalysts with enhanced coke resistance: Current status and perspective, *Catal. Today*, Vol. 256, pp. 29–40, 2015.
- [158] Li, Z.-H., Tian, S. X., Wang, H. T., and Tian, H. B., Plasma treatment of Ni catalyst via a corona discharge, *J. Mol. Catal. A: Chemical*, Vol. 211, pp. 149–153, 2004.
- [159] Banares, M. A., *Operando* methodology: combination of in situ spectroscopy and simultaneous activity measurements under catalytic reaction conditions, *Catal. Today*, Vol. 100, pp. 71–77, 2005.
- [160] Zhang, Y., Fu, D., Xu, X., Sheng, Y., Xu, J., and Han, Y.F., Application of operando spectroscopy on catalytic reactions, *Current Opinion in Chem. Eng.*, Vol. 12, pp. 1–7, 2016.
- [161] Bergmann, A. and Cuenya, B. R., Operando insights into nanoparticle transformations during catalysis, *ACS Catalysis*, Vol. 9, pp. 10020–10043, 2019.
- [162] Vamvakeros, A., Jacques, S. D. M., Michiel, M. D., Matras, D., Middelkoop, V., Ismagilov, I. Z., Matus, E. V., Kuznetsov, V. V., Drnec, J., Senecal, P., and Beale, A. M., 5D operando tomographic diffraction imaging of a catalyst bed, *Nature Commun.*, Vol. 9, pp. 4751, 2018.
- [163] Gibson, E. K., Stere, C. E., Curran-McAteer, B., Jones, W., Cibin, G., Gianolio, D., Goguet, A., Wells, P. P., Catlow, C. R. A., Collier, P., Hinde, P., and Hardacre, C., Probing the role of a non-thermal plasma (NTP) in the hybrid NTP catalytic oxidation of methane, *Angew. Chem. Int. Ed.*, Vol. 56, pp. 9351–9355, 2017.
- [164] Turan, N., Barboun, P. M., Nayak, P. K., Hicks, J. C., and Go, D. B., Development of a small-scale helical surface dielectric barrier discharge for characterizing plasma–surface interfaces, *J. Phys. D: Appl. Phys.*, Vol. 53 (27), pp. 275201, 2020.
- [165] Rivallan, M., Fourre, E., Aiello, S., Tatibouet, J.-M., and Thibault-Starzyk, F., Insights into the mechanisms of isopropanol conversion on  $\gamma$ -Al<sub>2</sub>O<sub>3</sub> by dielectric barrier discharge, *Plasma Process. Polym.*, Vol. 9, pp. 850–854, 2012.
- [166] Knoll, A. J., Zhang, S., Lai, M., Luan, P., and Oehrlein, G. S., Infrared studies of gas phase and surface processes of the enhancement of catalytic methane decomposition by low temperature plasma, *J. Phys. D: Appl. Phys.*, Vol. 52 (22), pp. 225201, 2019.

- [167] Stere, C. E., Adress, W., Burch, R., Chansai, S., Goguet, A., Graham, W. G., and Hardacre, C., Probing a non-thermal plasma activated heterogeneously catalyzed reaction using in situ DRIFTS-MS, *ACS Catalysis*, Vol. 5 (2), pp. 956–964, 2015.
- [168] Sheng, Z., Kim, H. H., Yao, S., and Nozaki, T., Plasma-chemical promotion of catalysis for CH<sub>4</sub> dry reforming: unveiling plasma-enabled reaction mechanisms, *Phys. Chem. Chem. Phys.*, Vol. 22, pp. 19349–19358, 2020.
- [169] Rodrigues, A., Tatibouet, J. M., and Fourre, E., Operando DRIFT spectroscopy characterization of intermediate species on catalysts surface in VOC removal from air by non-thermal plasma assisted catalysis, *Plasma Chem. Plasma Proc.*, Vol. 36 (4), pp. 901–915, 2016.
- [170] Lu, H., Yao, X., Li, J., Yao, S., Wua, Z., Zhang, H., Lin, H., and Nozaki, T., Mechanism on the plasma-catalytic oxidation of graphitic carbon over Au/ $\gamma$ -Al<sub>2</sub>O<sub>3</sub> by in situ plasma DRIFTS-mass spectrometer, *J. Hazard. Materials*, Vol. 396, pp. 122730, 2020.
- [171] Fridman, A. A. and Rusanov, V. D., Theoretical basis of non-equilibrium near atmospheric pressure plasma chemistry, *Pure & Appl. Chem.*, Vol. 66 (6), pp. 1267–1274, 1994.
- [172] Teramoto, Y. and Kim, H.-H., Effect of vibrationally excited N<sub>2</sub>( $\nu$ ) on atomic nitrogen generation using two consecutive pulse corona discharges under atmospheric pressure N<sub>2</sub>, *J. Phys. D: Appl. Phys.*, Vol. 52 (49), pp. 494003, 2019.
- [173] Qin, Y., Niu, G., Wang, X., Luo, D., and Duan, Y., Status of CO<sub>2</sub> conversion using microwave plasma, *J. CO<sub>2</sub> Util.*, Vol. 28, pp. 283–291, 2018.
- [174] Rusanov, V. D., Fridman, A. A., and Sholin, G. V., The physics of a chemically active plasma with nonequilibrium vibrational excitation of molecules, *Sov. Phys. Uspekhi*, Vol. 24 (6), pp. 447–474, 1981.
- [175] Berthelot, A. and Bogaerts, A., Modeling of CO<sub>2</sub> splitting in a microwave plasma: How to improve the conversion and energy efficiency, *J. Phys. Chem. C*, Vol. 121 (15), pp. 8236–8251, 2017.
- [176] Kozák, T. and Bogaerts, A., Splitting of CO<sub>2</sub> by vibrational excitation in non-equilibrium plasmas: a reaction kinetics model, *Plasma Source Sci. Technol.*, Vol. 23 (4), pp. 045004, 2014.
- [177] Snoeckx, R. and Bogaerts, A., Plasma technology - a novel solution for CO<sub>2</sub> conversion?, *Chem. Soc. Rev.*, Vol. 46, pp. 5805–5863, 2017.
- [178] Adrianto, D., Sheng, Z., and Nozaki, T., Mechanistic study on nonthermal plasma conversion of CO<sub>2</sub>, *Int. J. Plasma Environ. Sci. Technol.*, Vol. 14, pp. e01003, 2020.
- [179] Yamazaki, M., Nishiyama, S., and Sasaki, K., Decomposition of carbon dioxide by recombining hydrogen plasma with ultralow electron temperature, *Appl. Phys. Express*, Vol. 11 (6), pp. 066202, 2018.
- [180] Penetrante, B. M., Bardsley, J. N., and Hsiao, M. C., Kinetic analysis of non-thermal plasmas used for pollution control, *Jpn. J. Appl. Phys.*, Vol. 36, pp. 5007–5017, 1997.
- [181] Oh, J., Lim, H., Arafune, R., Jung, J., Kawai, M., and Kim, Y., Lateral hopping of CO on Ag(110) by multiple overtone excitation, *Phys. Rev. Lett.*, Vol. 116, pp. 056101, 2016.
- [182] Juurlink, L. B. F., McCabe, P. R., Smith, R. R., DiCologero, C. L., and Utz, A. L., Eigenstate-resolved studies of gas-surface reactivity: CH<sub>4</sub> ( $\nu_3$ ) dissociation of Ni (100), *Phys. Rev. Lett.*, Vol. 83 (4), pp. 868–871, 1999.
- [183] Juurlink, L. B. F., Killelea, D. R., and Utz, A. L., State-resolved probes of methane dissociation dynamics, *Progress in Surface Science*, Vol. 84 (3–4), pp. 69–134, 2009.
- [184] Smith, R. R., Killelea, D. R., DelSesto, D. F., and Utz, A. L., Preference for vibrational over translational energy in a gas-surface reaction, *Science*, Vol. 304, pp. 992–995, 2004.
- [185] Bisson, R., Sacchi, M., Dang, T. T., Yoder, B., Maroni, P., and Beck, R. D., State-resolved reactivity of CH<sub>4</sub>( $2\nu_3$ ) on Pt(111) and Ni(111): Effects of barrier height and transition state location, *J. Phys. Chem. A*, Vol. 111, pp. 12679–12683, 2007.
- [186] Ueta, H., Chen, L., Beck, R. D., Colón-Díaz, I., and Jackson, B., Quantum state-resolved CH<sub>4</sub> dissociation on Pt(111): coverage dependent barrier heights from experiment and density functional theory, *Phys. Chem. Chem. Phys.*, Vol. 15, pp. 20526–20535, 2013.
- [187] Kameshima, S., Tamura, K., Mizukami, R., Yamazaki, T., and Nozaki, T., Parametric analysis of plasma - assisted pulsed dry methane reforming over Ni/Al<sub>2</sub>O<sub>3</sub> catalyst, *Plasma Process. Polym.*, Vol. 14 (6), pp. 1600096, 2017.
- [188] Quan, J., Muttaqien, F., Kondo, T., Kozarashi, T., Mogi, T., Imabayashi, T., Hamamoto, Y., Inagaki, K., Hamada, I., Morikawa, Y., and Nakamura, J., Vibration-driven reaction of CO<sub>2</sub> on Cu surfaces via Eley-Rideal type mechanism, *Nature Chem.*, Vol. 11, pp. 722–729, 2019.
- [189] Kim, H. H., Ogata, A., and Futamura, S., Oxygen partial pressure-dependent behavior of various catalysts for the total oxidation of VOCs using cycled system of adsorption and oxygen plasma, *Appl. Catal. B: Environ.*, Vol. 79, pp. 356–367, 2008.
- [190] Kitano, M., Inoue, Y., Yamazaki, Y., Hayashi, F., Kanbara, S., Matsuishi, S., Yokoyama, T., Kim, S. W., Hara, M., and Hosono, H., Ammonia synthesis using a stable electride as an electron donor and reversible hydrogen store, *Nature Chem.*, Vol. 4, pp. 934–940, 2012.
- [191] Kanbara, S., Kitano, M., Inoue, Y., Yokoyama, T., Hara, M., and Hosono, H., Mechanism switching of ammonia synthesis over Ru-loaded electride catalyst at metal-insulator transition, *J. Am. Chem. Soc.*, Vol. 137 (45), pp. 14517–14524, 2015.

- [192] Sato, K., Imamura, K., Kawano, Y., Miyahara, S., Yamamoto, T., Matsunura, S., and Nagaoka, K., A low-crystalline ruthenium nano-layer supported on praseodymium oxide as an active catalyst for ammonia synthesis, *Chem. Sci.*, Vol. 8, pp. 674–679, 2017.
- [193] You, Z., Inazu, K., Aika, K., and Baba, T., Electronic and structural promotion of barium hexaaluminate as a ruthenium catalyst support for ammonia synthesis, *J. Catal.*, Vol. 251, pp. 321–331, 2007.
- [194] Kitano, M., Inoue, Y., Sasase, M., Kishida, K., Kobayashi, Y., Nishiyama, K., Tada, T., Kawamura, S., Yokoyama, T., Hara, M., and Hosono, H., Self-organized ruthenium–barium core–shell nanoparticles on a mesoporous calcium amide matrix for efficient low-temperature ammonia synthesis, *Angew. Chem. Int.*, Vol. 57, pp. 2648–2652, 2018.
- [195] Ogura, Y., Sato, K., Miyahara, S., Kawano, Y., Toriyama, T., Yamamoto, T., Matsumura, S., Hosokawa, S., and Nagaoka, K., Efficient ammonia synthesis over a Ru/La<sub>0.5</sub>Ce<sub>0.5</sub>O<sub>1.75</sub> catalyst pre-reduced at high temperature, *Chem. Sci.*, Vol. 9, pp. 2230–2237, 2018.
- [196] Kim, H. H., Teramoto, Y., Ogata, A., Takagi, H., and Nanba, T., Atmospheric-pressure nonthermal plasma synthesis of ammonia over ruthenium catalysts, *Plasma Process. Polym.*, Vol. 14 (6), pp. 1600157, 2017.
- [197] Barboun, P., Mehta, P., Herrera, F. A., Go, D. B., Schneider, W. F., and Hicks, J. C., Distinguishing plasma contributions to catalyst performance in plasma-assisted ammonia synthesis, *ACS Sustainable Chem. Eng.*, Vol. 7, pp. 8621–8630, 2019.
- [198] Li, S., Raak, T. v., and Gallucci, F., Investigating the operation parameters for ammonia synthesis in dielectric barrier discharge reactors, *J. Phys. D: Appl. Phys.*, Vol. 53 (1), pp. 014008, 2020.
- [199] Rouwenhorst, K. H. R., Kim, H.-H., and Lefferts, L., Vibrationally Excited Activation of N<sub>2</sub> in Plasma-Enhanced Catalytic Ammonia Synthesis: A Kinetic Analysis, *ACS Sustainable Chem. Eng.*, Vol. 7 (20), pp. 17515–17522, 2019.
- [200] Manabe, R., Nakatsubo, H., Gondo, A., Murakami, K., Ogo, S., Tsuneki, H., Ikeda, M., Ishikawa, A., Nakaicd, H., and Sekine, Y., Electrocatalytic synthesis of ammonia by surface proton hopping, *Chem. Sci.*, Vol. 8, pp. 5434–5439, 2017.
- [201] Ye, T.-N., Park, S.-W., Lu, Y., Li, J., Sasase, M., Kitano, M., Tada, T., and Hosono, H., Vacancy-enabled N<sub>2</sub> activation for ammonia synthesis on an Ni-loaded catalyst, *Nature*, Vol. 583, pp. 391–395, 2020.
- [202] Hayashi, F., Kitano, M., Yokoyama, T., Hara, M., and Hosono, H., Surface treatment for conductive 12 CaO·7Al<sub>2</sub>O<sub>3</sub> electride powder by rapid thermal annealing processing and its application to ammonia synthesis, *ChemCatChem*, Vol. 6 (5), pp. 1317–1323, 2014.
- [203] Murakami, K., Manabe, R., Nakatsubo, H., Yabe, T., Ogo, S., and Sekine, Y., Elucidation of the role of electric field on low temperature ammonia synthesis using isotopes, *Catal. Today*, Vol. 303, pp. 271–275, 2018.
- [204] Xu, S., Chansai, S., Shao, Y., Xu, S., Wang, Y. C., Haigh, S., Mu, Y., Jiao, Y., Stere, C. E., Chen, H., Fan, X., and Hardacre, C., Mechanistic study of non-thermal plasma assisted CO<sub>2</sub> hydrogenation over Ru supported on MgAl layered double hydroxide, *Appl. Catal. B: Environ.*, Vol. 268, pp. 118752, 2020.
- [205] Kim, J., Go, D. B., and Hicks, J. C., Synergistic effects of plasma–catalyst interactions for CH<sub>4</sub> activation, *Phys. Chem. Chem. Phys.*, Vol. 19, pp. 13010, 2017.
- [206] Mehta, P., Barboun, P. M., Engelmann, Y., Go, D. B., Bogaerts, A., Schneider, W. F., and Hicks, J. C., Plasma-catalytic ammonia synthesis beyond the equilibrium limit, *ACS Catalysis*, Vol. 10 (12), pp. 6726–6734, 2020.
- [207] Rouwenhorst, K. H. R., Burbach, H. G. B., Vogel, D. W., Pauli, J. N., Geerdink, B., and Lefferts, L., Plasma-catalytic ammonia synthesis beyond thermal equilibrium on Ru-based catalysts in nonthermal plasma, *Catal. Sci. Technol.*, Vol., pp. 2021.
- [208] Sheng, Z., Watanabe, Y., Kim, H. H., Yao, S., and Nozaki, T., Plasma-enabled mode-selective activation of CH<sub>4</sub> for dry reforming: First touch on the kinetic analysis, *Chem. Eng. J.*, Vol. 399, pp. 125751, 2020.
- [209] Nozaki, T., Tsukijihara, H., Fukui, W., and Okazaki, K., Kinetic analysis of the catalyst and nonthermal plasma hybrid reaction for methane steam reforming, *Energy & Fuel*, Vol. 21 (5), pp. 2525–2530, 2017.
- [210] Kang, W. S., Park, J. M., Kim, Y. H., and Hong, S. H., Numerical study on influences of barrier arrangements on dielectric barrier discharge characteristics, *IEEE Trans. Plasma Sci.*, Vol. 31 (4), pp. 504–510, 2003.
- [211] Kang, W. S., Hur, M., Song, Y. H., and Hong, S. H., Numerical simulation of atmospheric-pressure non-equilibrium plasmas: status and prospects, *Int. J. Plasma Environ. Sci. Technol.*, Vol. 7 (2), pp. 104–106, 2013.
- [212] Kang, W. S., Kim, H. H., Teramoto, Y., Ogata, A., Lee, J. Y., Kim, D.-W., Hur, M., and Song, Y.-H., Surface streamer propagations on an alumina bead: experimental observation and numerical modeling, *Plasma Sources Sci. Technol.*, Vol. 27 (1), pp. 015018, 2018.
- [213] Kim, H. H., Teramoto, Y., Ogata, A., Kang, W. S., Hur, M., and Song, Y. H., Negative surface streamers propagating on TiO<sub>2</sub> and  $\gamma$ -Al<sub>2</sub>O<sub>3</sub>-supported Ag catalysts: ICCD imaging and modeling study, *J. Phys. D: Appl. Phys.*, Vol. 51 (24), pp. 244006, 2018.
- [214] Kruszelnicki, J., Engeling, K. W., Foster, J. E., and Kushner, M. J., Interactions between atmospheric pressure plasmas and metallic catalyst particles in packed bed reactors, *J. Phys. D: Appl. Phys.*, Vol. 54 (10), pp. 104001, 2021.
- [215] Laer, K. V. and Bogaerts, A., Fluid modelling of a packed bed dielectric barrier discharge plasma reactor, *Plasma Sources Sci. Technol.*, Vol. 25 (1), pp. 015002, 2016.

- [216] Engeling, K. W., Kruszelnicki, J., Kushner, M. J., and Foster, J. E., Time-resolved evolution of microdischarges, surface ionization waves and plasma propagation in a two-dimensional packed bed reactor, *Plasma Sources Sci. Technol.*, Vol. 27 (8), pp. 085002, 2018.
- [217] Kruszelnicki, J., Engeling, K. W., Foster, J. E., Xiong, Z., and Kushner, M. J., Propagation of negative electrical discharges through 2-dimensional packed bed reactors, *J. Phys. D: Appl. Phys.*, Vol. 50 (2), pp. 025203, 2017.
- [218] Shirazi, M., Neyts, E. C., and Bogaerts, A., DFT study of Ni-catalyzed plasma dry reforming of methane, *Appl. Catal. B: Environ.*, Vol. 205, pp. 605–614, 2017.
- [219] Zhang, Y., Wang, H., Jiang, W., and Bogaerts, A., Two-dimensional particle-in cell/Monte Carlo simulations of a packed-bed dielectric barrier discharge in air at atmospheric pressure, *New J. Phys.*, Vol. 17, pp. 083056, 2015.
- [220] Somers, W., Bogaerts, A., Duin, A. C. T. v., and Neyts, E. C., Plasma species interacting with nickel surfaces: Towards an atomic scale understanding of plasma-catalysis, *J. Phys. Chem. C*, Vol. 116 (39), pp. 20958–20965, 2012.
- [221] Jafarzadeh, A., Bal, K. M., Bogaerts, A., and Neyts, E. C., CO<sub>2</sub> activation on TiO<sub>2</sub>-supported Cu<sub>5</sub> and Ni<sub>5</sub> nanoclusters: Effect of plasma-induced surface charging, *J. Phys. Chem. C*, Vol. 123 (11), pp. 6516–6525, 2019.